what happens as M continues to grow. By careful limiting arguments, we may indeed show that as M increases without bound the probability of symbol error will be arbitrarily small as long as E_b/N_0 exceeds $\log_e 2 = -1.6$ dB, the channel capacity limit for the infinite dimensionality channel developed in Section 2.9. (The interested reader is invited to pursue the derivation of this result in Exercises 3.3.9 and 3.3.10.) Thus, orthogonal signaling represents the first constructive signaling scheme we have encountered that operates arbitrarily near channel capacity for the infinite-bandwidth AWGN channel. However, it cannot be said to represent a practical solution to this objective for two reasons. First, the complexity, measured by the number of correlations needed per bit transmitted, grows as $M/\log_2 M$, and this is relatively large already for $M = 64$. Likewise, the dimensionality of the signal set, per bit transmitted, grows at the same rate, and thus orthogonal sets imply very large bandwidth. Referring to Figure 3.3.17, we see that, even for $M = 64$, the E_b/N_0 needed to achieve $P_s = 10^{-5}$ is roughly 6.5 dB, still some 8 dB away from the capacity limit, although this is a sizable improvement over *binary* orthogonal signaling.

If the messages to be communicated are actually just binary data, with M-ary signaling used to transmit m bits per symbol, where $M = 2^m$, then bit error probability, P_b, may be of more interest than the symbol error probability. For orthogonal signaling, these two are easily related combinatorially. Given that an error is made, then the $M - 1$ incorrect choices are equally likely, by symmetry of the signal space. Consider any bit position in the m-vector that labels signals, say the first position. Of the $M - 1$ error possibilities, exactly $M/2$ differ in the first (or any) bit position, and thus

$$P_b = \frac{M}{2(M-1)} P_s. \tag{3.3.41}$$

For large M, P_b approaches $P_s/2$. In fact, for any M we have the bounds

$$\frac{P_s}{2} < P_b \leq P_s, \tag{3.3.42}$$

so that bit error probability curves are only marginally different from symbol error probability curves at typical error rates.

M-ary Biorthogonal Case

Closely related to orthogonal signal sets are ***biorthogonal*** sets, obtained from the former by augmenting with the negatives of the signals. Thus, an M-ary biorthogonal set can be viewed as the union of an $(M/2)$-ary orthogonal set $\{s_i(t), i = 0, 1, \ldots, (M/2) - 1\}$ and the complementary set $\{-s_i(t)\}$. Demodulation is accomplished by correlating with all members of either orthogonal set and then finding the signal with the largest *magnitude*. The sign of this correlation reveals whether the decision should be in favor of an index in the correlating set or an index in the complementary set. Figure 3.3.18 depicts the receiver structure.

The principal advantages of such a construction relative to the orthogonal case are the following:

1. The number of correlators or matched filters needed to implement the optimal receiver for biorthogonal signals is only $M/2$.
2. The signal-space dimensionality is $M/2$, implying half the spectral bandwidth that a similar orthogonal construction requires.

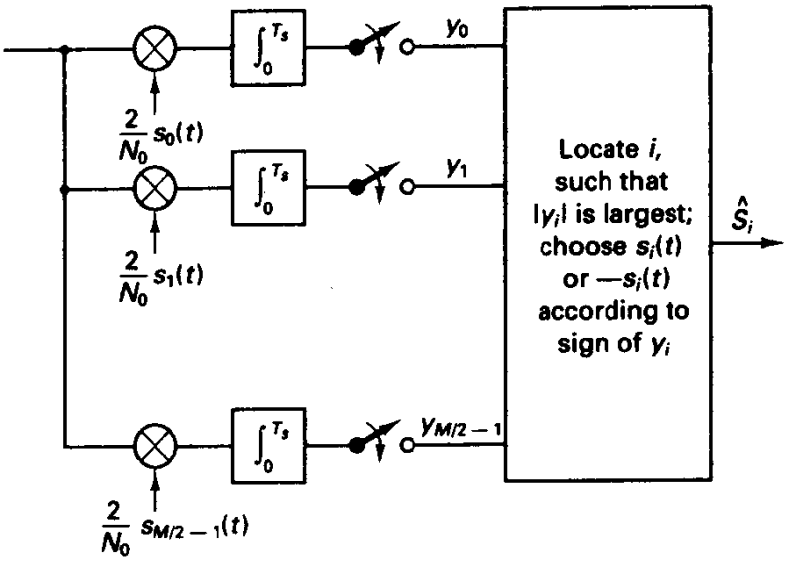

Figure 3.3.18 Biorthogonal receiver (note $M/2$ channels).

3. We gain in energy efficiency over the orthogonal design, much like binary antipodal is more efficient than binary orthogonal. (For M large, however, the saving is minor.)

To evaluate performance, we again assume that message S_0 is transmitted. Then our decision is correct if $y_0 > 0$ *and* $|y_i| < y_0$ for all $i = 1, 2, \ldots, (M/2) - 1$. Recall again that the r.v. Y_0 is Gaussian with $m = 2E_s/N_0$ *and* $\sigma^2 = 2E_s/N_0$. Also, $Y_i, i \neq 0$, are Gaussian with zero-mean, but the same variance as before, and are jointly independent; so we have that the probability of correct decision is

$$\begin{aligned} P(C) &= \int_0^{\infty} f(y_0|S_0) \left[\int_{-y_0}^{y_0} f(y_i|S_0)\, dy_i \right]^{(M/2)-1} dy_0 \\ &= \int_0^{\infty} \frac{e^{-(y_0-m)^2/2\sigma^2}}{(2\pi\sigma^2)^{1/2}} [1 - 2Q(y_0/\sigma)]^{(M/2)-1}\, dy_0. \end{aligned} \tag{3.3.43}$$

Again, we must resort to numerical integration. The symbol error probability $P_s = 1 - P(C)$, is shown in Figure 3.3.19 as a function of E_b/N_0 for varying M. Tables are found in [12] as well.

Once again we find that as M increases the energy efficiency improves steadily, and comparison of Figures 3.3.17 and 3.3.19 will reveal that biorthogonal sets are superior for all M, especially so for smaller M. Given the advantages we just cited for biorthogonal signaling, there now may seem to be no justification for selecting orthogonal designs. However, we have implicitly required with biorthogonal signaling the ability of the receiver to distinguish $s_i(t)$ from its complement, which in the carrier modulation case implies a phase synchronization operation. As we will see in Section 3.4, orthogonal signals may be detected noncoherently (without phase synchronization) with only minor energy penalty. Furthermore, it may simply be infeasible to physically realize the complement of one signal. An example is optical communication, where orthogonal

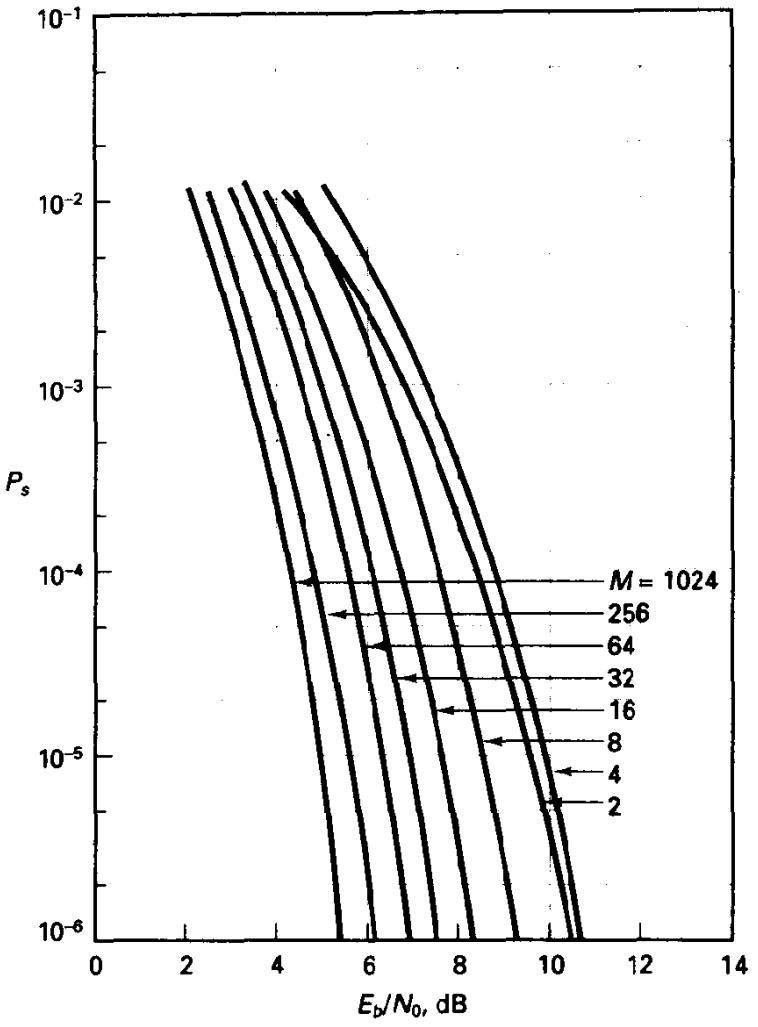

Figure 3.3.19 Symbol error probability for coherent detection of biorthogonal signals.

PPM is relatively easy to implement by pulsing a laser on or off, but synthesizing the negative of one of these pulse signals; that is, achieving a 180° optical phase shift, is more difficult.

Regarding the bit error probability for biorthogonal signaling, we note that there are now two types of error events, conditioned upon transmission of message S_0:

Case 1: Choosing $-S_0$ rather than S_0 (one possible event)

Case 2: Choosing one of the $M - 2$ signals orthogonal to S_0

Conventional bit labeling would assign the antipodal signal pairs with complementary bit labels. If case 1 occurs, all bits are decided incorrectly, but given the relatively large signal-space distance between antipodal pairs, it should be clear that this case is relatively rare. For case 2 situations, there are $M - 2$ equally likely decision errors, and, of these, $(M - 2)/2$ have bit discrepancies with S_0 in any given position. At all

reasonable signal-to-noise ratios, the case 2 events are far more probable. Thus, for M large, we again have that P_b approaches $P_s/2$. In any case, the upper and lower bounds of (3.3.42) remain valid.

M-ary Simplex Case

A ***simplex*** design, sometimes called a transorthogonal signal set, is obtained from an orthogonal set by translating the M-dimensional constellation so that its center of mass is at the origin and then realizing that the new constellation can be rotated into an $(M-1)$-dimensional coordinate system. Translation and rotation do not affect the probability of decision error, but can reduce the energy requirements slightly, in addition to reducing the signal dimensionality per bit.

Letting $\mathbf{s}_i$ denote the orthogonal set signal-space coordinates and $\mathbf{s}_i'$ denote the translated coordinates, we have (prior to final rotation)

$$\mathbf{s}_i' = \mathbf{s}_i - \frac{1}{M}\sum_{j=0}^{M-1}\mathbf{s}_j. \tag{3.3.44}$$

For $M = 2$, the simplex constellation is the antipodal design; for $M = 3$, the simplex constellation is formed by the vertices of an equilateral triangle; for $M = 4$, the simplex constellation is formed by the vertices of a regular tetrahedron; and so on.

By taking the Euclidean norm of each vector in (3.3.44), we can show that each new signal has energy given by $E_s' = E_s(M-1)/M$ (Exercise 3.3.12). Hence, with this simple energy correction, orthogonal signaling performance results may be used to evaluate simplex designs.

Another interesting property of the simplex design is that the normalized correlation between signals, which is equivalent to the normalized inner product in signal space, is

$$\lambda_{ij} = \frac{\mathbf{s}_i \cdot \mathbf{s}_j^T}{(E_{s_i}E_{s_j})^{1/2}} = \frac{-1}{M-1}, \tag{3.3.45}$$

which is the algebraically smallest correlation that can be *uniformly achieved* over an M-ary set of waveforms. If we view negative correlation as a useful attribute in deciding between *two signals*, the simplex would seem to provide an optimal (minimum error probability) signal design for a given M and E_s/N_0, when dimensionality is unconstrained. The strong simplex conjecture, that the simplex provides the minimum error probability signal set under an average power constraint for the AWGN channel, has recently been invalidated by Steiner [18]. However, the construction does supply the set with largest minimum distance between signal points and minimizes the union bound on error probability under an average energy constraint. With all signals constrained to have equal energy, it is still conjectural that the simplex minimizes error probability at any SNR.

We conclude the discussion of orthogonal, biorthogonal, and simplex sets with an example for $M = 8$.

Example 3.6 $M = 8$ with Fixed E_b/N_0

Suppose a communication system operating over an AWGN channel can supply $E_b/N_0 = 5$ dB $= 3.16$. We consider 8-ary signaling, which means that, should we require it,

$E_s/N_0 = 3.16$ ($\log_2 8$) $= 9.48$ or 9.8 dB. Reference to Figures 3.3.17 and 3.3.19 produces $P_s = 6.5 \cdot 10^{-3}$ and $5.8 \cdot 10^{-3}$, respectively, for orthogonal and biorthogonal designs. An 8-ary simplex can be evaluated by entering the orthogonal curves at $\frac{8}{7}$ times the available E_b/N_0, producing $P_s \doteq 3.0 \cdot 10^{-3}$.

To form the signal set, we might utilize the Hadamard construction. The Hadamard matrix of order 4 is

$$\mathbf{H}_4 = \begin{bmatrix} \mathbf{H}_2 & \mathbf{H}_2 \\ \mathbf{H}_2 & -\mathbf{H}_2 \end{bmatrix} = \begin{bmatrix} 1 & 1 & 1 & 1 \\ 1 & -1 & 1 & -1 \\ 1 & 1 & -1 & -1 \\ 1 & -1 & -1 & 1 \end{bmatrix} \tag{3.3.46}$$

and these four rows plus their complements form an 8-ary biorthogonal set. The selected row could be sent as a rectangular pulse train having duration $T_s = T_b \log_2 M = 3T_b$.

The Hadamard matrix of order 8 is

$$\mathbf{H}_8 = \begin{bmatrix} \mathbf{H}_4 & \mathbf{H}_4 \\ \mathbf{H}_4 & -\mathbf{H}_4 \end{bmatrix}, \tag{3.3.47}$$

and its 8 rows are the chosen signal patterns for the 8-ary orthogonal set. Note that in the latter the first element in all rows is 1, meaning this signal element lends no distinguishability to the signal set and can be eliminated with no loss in performance. Doing so allows lowering of the energy per bit to $\frac{7}{8}$ of the former value, while maintaining $d_{\min}$ fixed and thus achieving the same error probability. Also, it is clear that the dimensionality of the set is reduced to seven (for example, we can use seven nonoverlapping pulses as the basis functions).

3.3.4 Detection of M-ary Phase Shift Keying (M-PSK)

M-PSK is perhaps the generic form of modulation most widely utilized in contemporary practice, ranging from voice-band modems to high-speed satellite transmission. As the name suggests, the signal set is generated by phase modulation of a sinusoidal carrier to one of M equispaced phase positions. The M signals are described by

$$s_i(t) = \left(\frac{2E_s}{T_s}\right)^{1/2} \cos\left(\omega_c t + \frac{2\pi i}{M}\right), \qquad i = 0, 1, \ldots, M-1, \quad 0 \le t \le T_s, \tag{3.3.48}$$

with E_s denoting the energy per symbol and ω_c denoting the carrier frequency in radians per second. As noted earlier, two basis functions are sufficient to generate this set:

$$\phi_0(t) = \left(\frac{2}{T_s}\right)^{1/2} \cos(\omega_c t) \quad \text{and} \quad \phi_1(t) = \left(\frac{2}{T_s}\right)^{1/2} \sin(\omega_c t). \tag{3.3.49}$$

If $M = 2$, we have ***binary phase shift keying*** (also BPSK or simply PSK), an example of an antipodal set. When $M = 4$, we refer to this modulation as ***quadriphase shift keying***,[12] which we observe also constitutes a biorthogonal set. For any M, the signal constellation consists of M points equally spaced on a circle of radius $E_s^{1/2}$.

[12] Also referred to as quadrature-phase-shift-keying, QPSK, or 4-PSK.

This modulation scheme, or minor variations of it, is frequently employed in practice for several reasons:

1. The signals are easily formed using discrete phase shifter technology; in the case of $M = 2$ and $M = 4$-PSK, the synthesis can be done by sign modulation of a carrier or quadrature versions of the carrier.
2. The signals have constant amplitude (at least if unfiltered) and therefore may be amplified by nonlinear devices without significant distortion penalty. Such nonlinear amplifiers are typically found in satellite and terrestrial power amplifiers in the form of traveling wave tubes, klystrons, and semiconductor amplifiers operated in saturated mode.
3. Bandwidth conservation is afforded if M is large, since the dimensionality per bit transmitted becomes smaller with increasing M. This is in exchange for an increased signal-to-noise ratio requirement, however.

The simplest form of the optimal demodulator is a two-channel correlator using phase-quadrature versions of a synchronized carrier reference (see Figure 3.3.2). The received waveform, $r(t)$, is projected into two-dimensional signal space, as shown in Figure 3.3.20, and decision regions (or nearest-neighbor zones) are pie-shaped sectors with angular extent $2\pi/M$ radians, centered on the various signal points. These regions are shown in Figure 3.3.20 for $M = 8$, called 8-PSK or octal PSK in the literature.

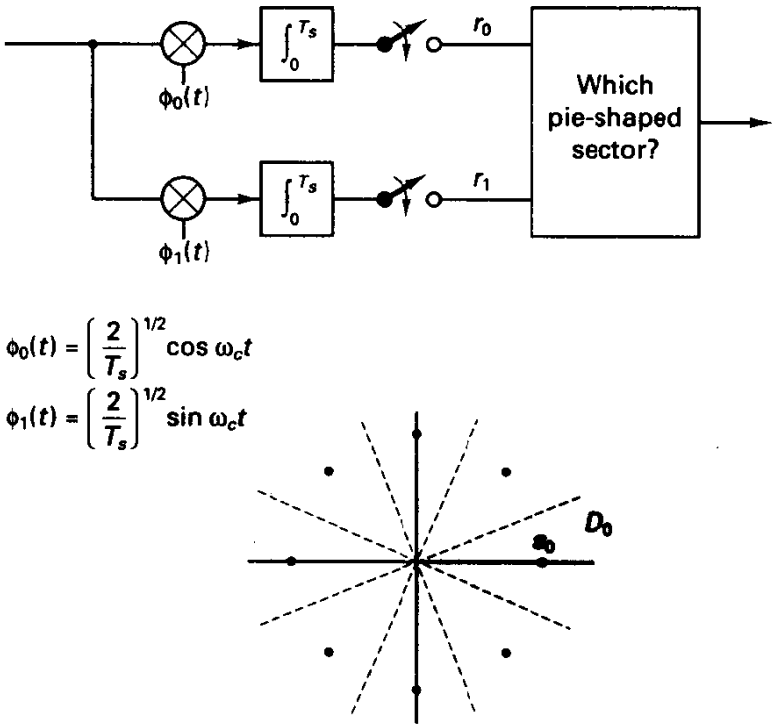

Figure 3.3.20 M-PSK demodulator in basis function form and decision zones for $M = 8$.

By inspection of the signal-space symmetry, the probability of correct decision, conditioned upon transmission of S_i, is independent of i. Thus, consider $P(C|S_0)$:

$$P(C|S_0) = P((R_0, R_1) \in D_0|S_0) = P(|R_1| < R_0 \tan(\pi/M)|S_0)$$
$$= 2\int_0^\infty \frac{e^{-(r_0-m)^2/\sigma^2}}{(2\pi\sigma^2)^{1/2}} \left(\int_0^{r_0 \tan(\pi/M)} \frac{e^{-r_1^2/2\sigma^2}}{(2\pi\sigma^2)^{1/2}} dr_1 \right) dr_0 = 1 - P_s, \tag{3.3.50}$$

where $m = E_s^{1/2}$ and $\sigma^2 = N_0/2$. For $M = 2$, this expression collapses to $P_s = Q[(2E_b/N_0)^{1/2}]$, as we earlier found for antipodal signaling. For larger M, we must resort to numerical integration of (3.3.50) or to bounding techniques. Numerical results are shown in Figure 3.3.21 for various M as a function of E_b/N_0, taken from tables in [12].

In sharp contrast to the situation with orthogonal signals, for M-PSK the required energy-to-noise-density ratio *increases with* M, which is not surprising if we realize that for every doubling of M the distance between points on the circle is approximately

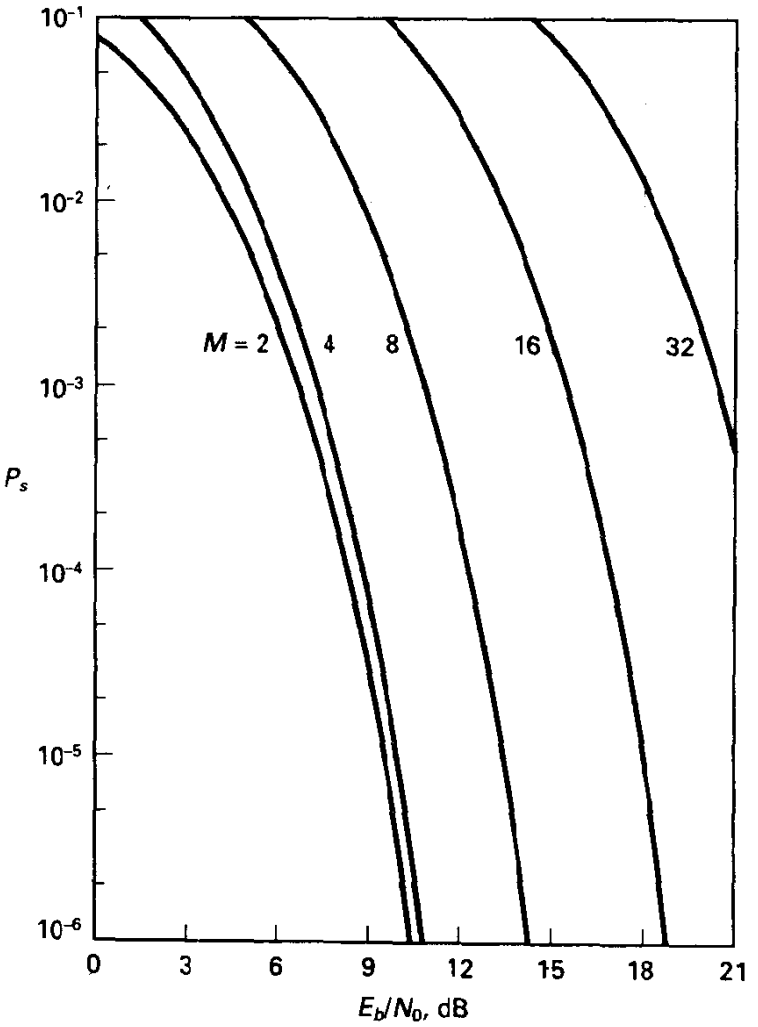

Figure 3.3.21 Symbol error probability for coherent detection of M-PSK.

halved, even after allowing for $E_s = E_b \log_2 M$. Thus, doubling of M projects a 6-dB loss in energy efficiency when M is large, and Figure 3.3.21 begins to reveal this trend.

The bounding procedures described in Section 3.3.2 can be easily and accurately applied to the M-PSK situation. The probability of symbol error is certainly greater than the probability of error in deciding between a given signal and one of its nearest neighbors. Since this distance is $2(E_s^{1/2}) \sin(\pi/M)$, we have from (3.3.28b) a lower bound:

$$P_s \geq Q\left[\left(\frac{2E_s}{N_0}\right)^{1/2} \sin\frac{\pi}{M}\right]. \tag{3.3.51a}$$

On the other hand, since D_i^c is the union of *two* half-spaces in two dimensions, each defined by a nearest-neighbor decision problem, we have an upper bound from (3.3.34):

$$P_s \leq 2Q\left[\left(\frac{2E_s}{N_0}\right)^{1/2} \sin\frac{\pi}{M}\right]. \tag{3.3.51b}$$

Expressing (3.3.51a) and (3.3.51b) in terms of E_b/N_0, we obtain

$$Q\left(\left[\frac{2E_b}{N_0}(\log_2 M)\sin^2\frac{\pi}{M}\right]^{1/2}\right) < P_s < 2Q\left(\left[\frac{2E_b}{N_0}(\log_2 M)\sin^2\frac{\pi}{M}\right]^{1/2}\right). \tag{3.3.52}$$

We have rather tightly bounded the true error probability to within a factor of 2, as was first shown by Arthurs and Dym [14]. Furthermore, at high signal-to-noise ratio, inspection of the error region would suggest that the upper bound is quite accurate, particularly so as M increases, since the doubly counted region in the plane becomes small. To demonstrate this, we consider $M = 8$ phase shift keying, with $E_b/N_0 = 10$ dB. In [12], the actual P_s from numerical integration of (3.3.50) is given as $3.03 \cdot 10^{-3}$. On the other hand, substitution into the upper bound (3.3.52) gives $P_s \leq 3.08 \cdot 10^{-3}$.

Equation (3.3.52) explicitly displays that the energy efficiency, relative to antipodal signaling, is

$$\eta_{\text{MPSK}} = (\log_2 M)\sin^2\frac{\pi}{M} \tag{3.3.53}$$

which drops by roughly 6 dB for every doubling of M, when M is large.

We may also be interested in the *bit error probability* associated with M-PSK transmission. In contrast to the situation for orthogonal signaling, the bit labeling is important to consider here, since certain error events are much more dominant than others. Specifically, the nearest-neighbor errors are the most likely, while the antipodal error events are very rare at high SNR. This suggests the use of Gray-coded labeling, wherein adjacent signal points have bit labels that differ in as few bits as possible, that is, one. It is possible to do this for any $M = 2^m$. Gray coding of 4-PSK and 8-PSK is listed in Figure 3.3.22.

Under the approximation that only adjacent symbol errors occur, which is increasingly true as E_s/N_0 increases, the bit error probability, P_b, can be taken to close approximation as $P_s/\log_2 M$, since adjacent errors induce only one bit error in $\log_2 M$ bit positions, and over uniform choice of transmitted signals, this bit error appears uniformly in all bit positions.

As a point of special interest, the *bit error probability* for 4-PSK is exactly the same as that of binary PSK when they are compared at equal E_b/N_0. This may be argued by

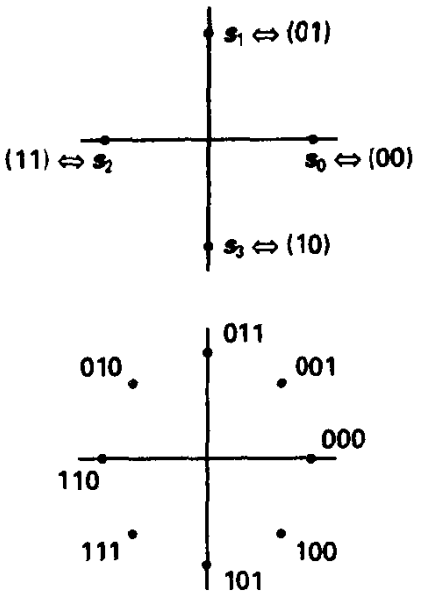

Figure 3.3.22 Gray-code labeling for $M = 4$ and $M = 8$ PSK.

realizing that with Gray coding, each information bit is resolved in a binary test of one half-plane against another. The distance to the decision boundary is $(E_s/2)^{1/2} = E_b^{1/2}$, giving

$$P_b = Q\left[\left(\frac{2E_b}{N_0}\right)^{1/2}\right], \quad \text{QPSK, Gray coded, AWGN} \tag{3.3.54}$$

Despite this equivalence in energy efficiency with binary PSK, 4-PSK signals occupy only half the spectrum that binary PSK occupies for a given bit rate,[13] producing one of those rare occurrences of something for (almost) nothing! Consequently, QPSK has become the base-line technique for a myriad of digital satellite systems. The only significant penalty factor is an increased sensitivity to carrier phase synchronization error.

Differential Encoding and Decoding of PSK

Demodulation of PSK signals as described presumes a synchronized local phase reference in the receiver, because information resides in the absolute phase angle of the carrier relative to $\omega_c t$ radians. Usually the carrier synchronization process has an M-fold ambiguity, that is, the phase estimate produced by the synchronizer can be the correct phase, or one or $M - 1$ equally likely other estimates spaced by $2\pi/M$ radians in phase angle. This can be disastrous for detection performance, even without the addition of noise. One possible solution is the periodic inclusion of a known pattern in the message sequence to resolve the ambiguity, but this is inconvenient

[13]This is because the orthogonal bases $\cos(\omega_c t)$ and $\sin(\omega_c t)$ can be independently modulated and occupy the same spectral region that modulation of either alone would occupy.

and consumes energy and bandwidth, so we consider a simple means to operate in the face of such possibilities, referred to as ***differential encoding and decoding***.

At the modulator, we let the current phase angle θ_n be determined recursively by

$$\theta_n = \theta_{n-1} + x_n \frac{2\pi}{M}, \quad \text{modulo } 2\pi, \tag{3.3.55}$$

where $x_n \in \{0, 1, \ldots, M-1\}$ is the modulator input at symbol time n. In essence, we let information reside in phase differences from symbol to symbol and utilize the difference of two consecutive (phase-ambiguous) symbol decisions in the receiver to form information decisions. The latter will be invariant to the actual synchronization state of the receiver, assuming the synchronizer does not slip synchronization states. Differential modulation induces a simple memory into the process, but it has no real consequence for energy efficiency or spectral shaping.

Example 3.7 4-ary Differential Encoding

We use 4-PSK as an example, and in Table 3.1 we list the encoding rule, which employs Gray coding of the phase *increments*.

TABLE 3.1 DIFFERENTIAL ENCODING RULE FOR 4-PSK

Information Symbol	Phase Change, radians
00	0
01	$\frac{\pi}{2}$
11	π
10	$\frac{3\pi}{2}$

Suppose the bit sequence 01, 11, 10 is to be sent, and the initial phase at the modulator is $\pi/2$ radians. Then the transmitted phase sequence over four symbols is $\pi/2, \pi, 0, 3\pi/2$, according to Table 3.1.

Upon reception of the noisy signal, the receiver may synchronize to any of four positions, but comparison of two consecutive decisions will produce the correct two information bits, at least assuming both decisions are correct. In effect, the unknown lock state of the synchronizer is self-canceling. Wu [15] shows in detail how to implement the encoding and decoding operations in logic gate form. For the binary case, differential encoding and decoding are especially simple (see Figure 3.3.23).

There is a small penalty for this convenience: if the predecoding symbol error rate is P_s, then at the output of the differential detector the error probability is $2P_s(1 - P_s)$, so typically the symbol error rate is approximately doubled. Also, paired errors are common in the output symbol stream, since one decision error affects two consecutive differential decisions. To make up for this doubling of error probability, however, only a fraction of a decibel in SNR must be added because of the strong sensitivity of error probability to SNR. At $P_s = 10^{-5}$, the energy penalty is only about 0.3 dB.

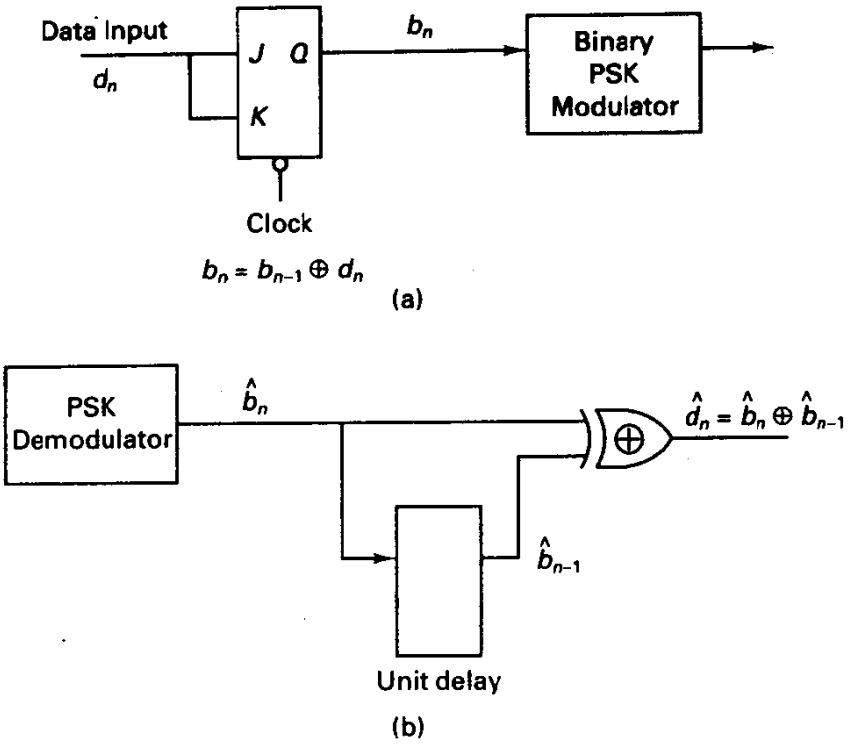

Figure 3.3.23 Binary differential encoding with J-K flip flop. (a) encoder; (b) decoder.

3.3.5 *M*-ary Amplitude Modulation and Quadrature Amplitude Modulation

When bandwidth efficiency is of primary importance, modulation schemes with small signal-space dimensionality per bit transmitted ($N/\log_2 M$) are necessary. M-PSK is one such alternative; for large M, however, arrangement of the M constellation points on a circle becomes progressively less energy efficient. If the channel exhibits good amplitude linearity, then ***M-level amplitude modulation*** (M-AM) and its extension to the amplitude modulation of phase-quadrature carriers are more efficient constellations. The latter is referred to as ***quadrature amplitude modulation*** (QAM) or M-ary AM/PM, for amplitude and phase modulation, and has become popular in voice-band data transmission [16] and in spectrally-efficient digital transmission on microwave channels [17].

Let's consider first the case of M-AM, with M even, wherein the transmitted signal is related to a data symbol $x_i \in \{0, 1, \ldots, M-1\}$ by

$$s_i(t) = (2x_i - M + 1)\phi(t) \tag{3.3.56}$$

and $\phi(t)$ is a common signal shape to all signals, either a baseband pulse or a burst of a carrier-frequency signal. Often this pulse shape is chosen for spectrum-shaping purposes. The set of (3.3.56) has been constructed so that the net amplitude modulation is symmetric about the zero level, which is the most energy-efficient design; however, unipolar modulation is possible as a variation.

With the symmetric signal set of (3.3.56), the signal-space constellation is the one-dimensional set pictured in Figure 3.3.24a. We first define the *spacing* between signal points (in signal space at the receiver) as $2a$, so the signal constellation points are located at $\pm a, \ldots \pm (M-1)a$. The energy levels of the various signals are $a^2, 9a^2, 25a^2, \ldots (M-1)^2a^2$. The average energy associated with this set is obtained by summing the squares of odd integers and averaging. This produces

$$E_s = \frac{(M^2-1)a^2}{3}, \tag{3.3.57}$$

which, as we expect, increases as the square of the number of modulator signals.[14]

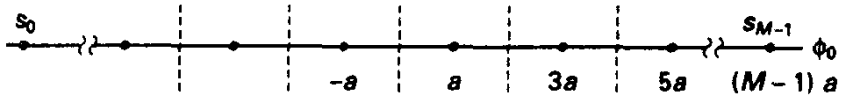

Figure 3.3.24a M-AM signal constellation and decision regions.

The optimal receiver is simplest in basis function form (Figure 3.3.24b), where we generate a scalar statistic and compare with a set of thresholds, $0, \pm a, \pm 2a$, and so on, to decide the index of the data symbol in accord with (3.3.56). Notice that in the M-AM (and the M-QAM case as well), the optimal receiver must know the scale factor for the received signal; otherwise, decision thresholds cannot be properly set. Some form of automatic gain control (AGC) is thus required in such demodulators.

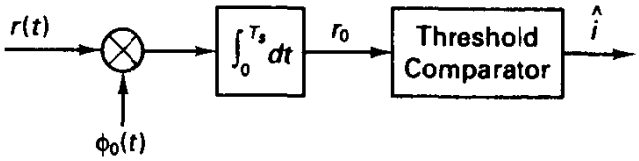

Figure 3.3.24b M-AM receiver.

For a unit-energy basis projection, the variance of the noise component is $N_0/2$, and the error probability for M-ary AM is given by the probability that zero-mean Gaussian noise with variance $N_0/2$ causes the statistic to be outside the proper decision zone. With reference to Figure 3.3.24c, and recalling that the probability of error for confusing two signals having intrasignal distance $d = 2a$, we find that inner constellation points have conditional error probability $2Q[d/(2N_0)^{1/2}]$, while the outer two points have conditional error probability $Q[d/(2N_0)^{1/2}]$. Thus, the symbol error

[14]This is nearly the same as the second moment of a uniform mass distribution on the same interval: $(M-1)^2a^2/3$.

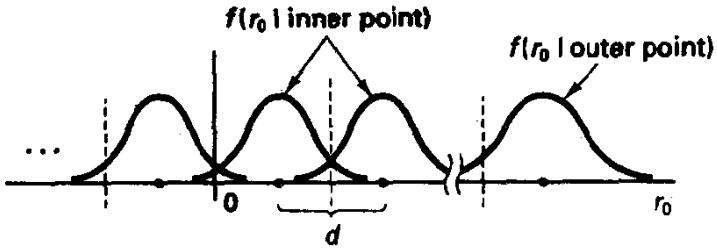

Figure 3.3.24c Conditional p.d.f.'s for various signal points.

probability is

$$\begin{aligned} P_s &= \frac{M-2}{M} P(\epsilon|\text{inner point}) + \frac{2}{M} P(\epsilon|\text{outer point}) \\ &= \frac{2(M-1)}{M} Q\left[\frac{d}{(2N_0)^{1/2}}\right] \\ &= \frac{2(M-1)}{M} Q\left[\left[\frac{6E_s}{(M^2-1)N_0}\right]^{1/2}\right] \\ &= \frac{2(M-1)}{M} Q\left[\left[\frac{2E_b}{N_0}\frac{3\log M}{M^2-1}\right]^{1/2}\right] \end{aligned} \tag{3.3.58}$$

since $E_s = E_b \log M$. Thus, overlooking a multiplier (which is less than 2), to obtain a given error probability, M-AM is a factor of $(3\log M)/(M^2-1)$ less efficient in energy utilization than binary antipodal signaling [compare (3.3.23)]. This is a substantial penalty for large M, but we improve spectral efficiency in proportion to $\log_2 M$, since $\log_2 M$ bits are sent per signal-space dimension.

To minimize bit error probability, Gray coding of the amplitude levels would be used, since nearest-neighbor errors are predominant, and the bit error probability can be approximated for large M by

$$\begin{aligned} P_b &\approx \frac{1}{\log M} P_s \\ &\approx \frac{2}{\log M} Q\left[\left[\frac{2E_b}{N_0}\frac{3\log M}{M^2-1}\right]^{1/2}\right]. \end{aligned} \tag{3.3.59}$$

We have already seen in the case of 4-PSK how quadrature modulation achieves a doubling of the spectral efficiency relative to that of 2-PSK, without any increase in required E_b/N_0. The same notion can be exploited here to perform quadrature amplitude modulation. If we simply modulate $\cos\omega_c t$ and $\sin\omega_c t$ each by 2^m equally spaced levels, as before, we obtain square constellations with $M = 2^{2m}$ points, which for $M = 4, 16, 64, 256, \ldots$, are reasonably efficient and simple to instrument. For intermediate values of M, say $32, 128, \ldots$, a cross-construction is easily implemented and efficient, in which we begin with a square constellation with $M/2$ points and

append on the periphery $M/2$ additional points in four zones. Figure 3.3.25 shows such constellations for $M = 16, 32, 64$, and 128. These arrangements of signal points are particularly convenient since the optimal decision zones, D_i, are rectangular with edges aligned along signal-space axes, and decision making reduces to separately thresholding each signal-space coordinate.

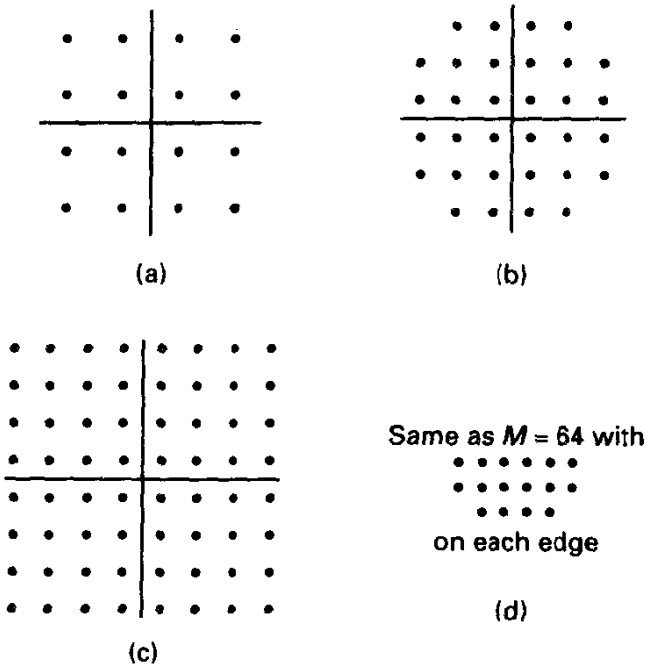

Figure 3.3.25 QAM constellations. (a) $M = 16$, three decision zones shaded; (b) $M = 32$; (c) $M = 64$; (d) $M = 128$.

Evaluation of the performance of QAM is a simple matter of calculating the average energy in terms of one-dimensional signal spacing $2a$ and bounding the error probability in terms of this same distance. In QAM, inner constellation points have four nearest neighbors, and the corresponding error region is the union of four half-spaces. Referring to Figure 3.3.25, we find, however, that edge points and corner points have three or two neighbors, respectively. (Figure 3.3.25 illustrates the three types of decision zones for different constellation points in 16-QAM.) An upper bound is obtained by assuming a multiplier of 4 for all cases:

$$P_s \leq 4Q\left[\frac{d}{(2N_0)^{1/2}}\right]. \tag{3.3.60}$$

This may always be converted into the form

$$P_s \leq 4Q\left[\left(\frac{2E_b}{N_0}\eta_M\right)^{1/2}\right], \tag{3.3.61}$$

where η_M is an efficiency factor, normalized to the efficiency of antipodal signaling, and depends on the constellation size and shape. For M-AM and M-QAM designs, we will find that $\eta_m \leq 1$. Figure 3.3.26 tabulates these efficiencies, for the QAM constellations. To illustrate calculation of these efficiencies, we consider the 32-point QAM cross-constellation.

M_{AM}	M_{QAM}	η_M, dB
4	16	−4.0
–	32	−6.0
8	64	−8.5
–	128	−10.2
16	256	−13.3

Figure 3.3.26 Relative energy efficiencies for M-AM and M-QAM, normalization is to antipodal design.

Example 3.8 Error Probability for 32-Point QAM

The 32-point constellation of Figure 3.3.25 is scaled to have signal spacing $d = 2a$ in each dimension. The various energies are $2a^2$, $10a^2$, $18a^2$, $26a^2$, and $34a^2$, with populations at these various energies of 4, 8, 4, 8, and 8, respectively. Assuming equiprobable selection, we determine that the average energy, expressed in terms of distance, is

$$E_s = 20a^2 = 5d^2 \tag{3.3.62}$$

so that $d = (E_s/5)^{1/2}$. Substitution into (3.3.60) and use of $E_s/N_0 = 5E_b/N_0$ produces

$$P_s \le 4Q\left[\left[\frac{2E_b}{N_0}\frac{1}{4}\right]^{1/2}\right] \tag{3.3.63}$$

indicating a relative efficiency of $10\log\left(\frac{1}{4}\right) = -6$ dB for 32-QAM relative to antipodal signaling.

Tighter bounding is possible in this case by counting nearest neighbors and averaging properly. It happens in this case that the multiplier of 4 can be reduced slightly to 3.5. The lower-bound multiplier can also be tightened by realizing that the complement of D_i is, except for corner points, partially covered by two nonoverlapping half-spaces, so the lower-bound multiplier can become essentially 2.

In the one-dimensional case, (3.3.58) reveals each doubling of M, or increasing the dimensional efficiency by one bit/dimension, necessitates roughly a factor of 4 (6 dB) increase in E_b/N_0 to maintain a given P_s. For two-dimensional QAM modulation, we may quadruple M in exchange for increasing signal-to-noise ratio by 6 dB, as shown by the tabulation of η_M in Figure 3.3.26. This increases dimensional efficiency by 2 bits/2 dimensions, so in this sense QAM apparently offers no intrinsic benefit over M-AM. We will see in our study of power spectra in Section 3.7, however, that the QAM format really does gain by a factor of 2 in spectral efficiency for the same energy efficiency, extending the superiority of QPSK over binary PSK. The reason is that the two sinusoidal basis functions really constitute only one complex signal dimension.

To minimize bit error probability, proper bit labeling should be made to ensure that adjacent signal points differ in as few bits as possible. For square constellations with $M = 2^{2m}$, this is achieved with Gray coding of m bits along each coordinate axis.

Example 3.9 Digital Microwave Transmission Using 64-QAM

As an application of QAM, consider transmission of binary data at rate $R_b = 90$ Mbps over a digital microwave radio link. The channel bandwidth allocation is 20 MHz in the 4-GHz region for this application, so we seek a transmission method that affords a large number of bits/dimension and adopt 64-QAM. Because we transmit $m = 6$ bits per symbol interval,

the required symbol rate is 15 Msps, and with proper choice of modulator pulse shape $g(t)$, the resulting power spectrum can meet the 20-MHz constraint. (More discussion on this topic follows later in the chapter.)

Let's suppose the required bit error probability must not exceed 10^{-5}. Using the approximation that a symbol error is most likely to produce one bit error among the six decoded bits, along with the efficiency factor for 64-QAM, we set

$$P_b = 10^{-5} \approx \frac{4}{6} Q\left[\left[\frac{2E_b}{N_0}\eta_{64}\right]^{1/2}\right] \tag{3.3.64}$$

and find the required $E_b/N_0 = 18.1$ dB.[15] Often cited instead is the required "signal-to-noise ratio" (SNR), which is (unfortunately) defined in several ways. A typical definition of SNR is the ratio of signal power to noise power, measured in a bandwidth equaling the symbol rate:

$$\text{SNR} = \frac{E_s/T_s}{N_0 R_s} = \frac{E_s}{N_0} = \left(\frac{E_b}{N_0}\right)\log_2 M. \tag{3.3.65}$$

Therefore, the theoretical SNR by this definition would need to be $18.1 + 10\log_{10} 6 = 25.9$ dB. The actual SNR to achieve the desired performance, as quoted by a manufacturer, may be several decibels larger due to the need to overcome impairments caused by intersymbol interference, multipath effects, nonlinear distortion of amplifiers, losses due to synchronization, and other impairments associated with the microwave channel.

As a note on technology, several manufacturers now supply 256-point QAM microwave digital radio equipment. This modulation is able to increase the bandwidth efficiency by a factor of $\frac{8}{6}$, in exchange for still larger required E_b/N_0. 1024-point QAM may be "just around the corner." The interested reader is referred to a discussion of digital microwave radio techniques found in [17].

3.3.6 Multidimensional Lattice-based Constellations for the AWGN Channel

We have just focused on large constellations of points in one- and two-dimensional signal spaces, formed by a simple arrangement of points on a one- or two-dimensional grid. The performance analysis for these cases raised the following signal design problem: locate M signal points in a one- or two-dimensional space so that the minimum intrasignal distance is some target value d, and so that the average energy of the constellation is minimized. (An alternative is to minimize the *peak* energy.)

It is natural to inquire whether we have done the best arrangement in one and two dimensions, as well as what potential exists in higher-dimensional signal spaces. The question is related to the classical sphere-packing problem [19], wherein we wish to pack N-dimensional balls having radius $d/2$ as densely as possible. This follows since decision regions for regularly arranged points whose separation in N-dimensional space is d are regions circumscribing spheres[16] of radius $d/2$. For one-dimensional signal constellations, the solution is obvious, and for the one just studied, place points equally spaced along the real line in signal space, symmetrically about the origin.

[15] Recall that antipodal signaling requires approximately $E_b/N_0 = 9.6$ dB.

[16] Sphere must be understood in a general sense here; for example, a two-dimensional sphere is a circle.

In two dimensions, we have found that placing points on the two-dimensional grid offers no intrinsic gain in packing efficiency over the one-dimensional arrangement, but there is a more dense regular arrangement of two-dimensional points. It is readily exhibited by arranging coins on the table, producing the hexagonal sphere-packing shown in Figure 3.3.27. Signal points are located at the vertices of equilateral triangles that tessellate the plane, and the nearest-neighbor decision zone (also called the Voronoi region) for each point is a hexagon; thus the term hexagonal packing. A simple volumetric comparison will show that this hexagonal packing is 15% more dense than the two-dimensional grid, or rectangular packing, meaning that in a given large area of the plane 15% more coins may be placed with the hexagonal arrangement than with the rectangular centering, keeping d constant. Since the average energy of a constellation is proportional to radius squared (we neglect the discreteness of the constellation here, as well as constellation edge effects), a given value of M may be attained with 15% less signal-space area, or 15% less energy to maintain the same intrasignal distance. This in turn projects a 0.6-dB increase in energy efficiency for the optimal packing. This is partially offset by an increase in the number of nearest neighbors from four to six.

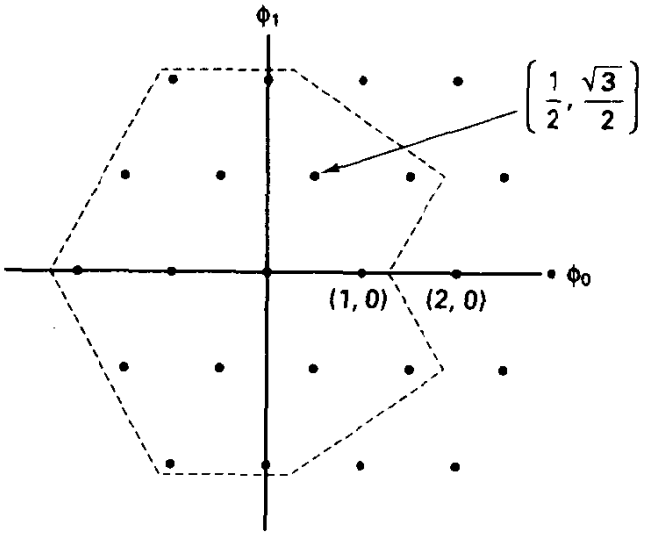

Figure 3.3.27 Section of hexagonal lattice with $M = 16$ points. Center of mass is $(-1/4, 0)$.

The practical problem with this two-dimensional packing is that it does not lead to convenient constellations for $M = 8, 16, 32, \ldots$, and the decision boundaries are no longer as simple as before. Foschini et al. [20] have studied hexagonal constellations, finding small (about 0.5 dB) gains for $M = 16$. Simon and Smith [21] also treat this signal design problem. Generally, the small gains available are not deemed worth the added complexity.

More interesting possibilities emerge in three or more dimensions. A systematic means of describing large sets of points in N-dimensional Euclidean space involves ***lattices*** [22]. For ease of modulator implementation and, more importantly, demodulation, lattice-based constellations are preferred over other more general arrangements, at least for large M. This is because fast procedures exist for finding the nearest point in a lattice to a received point in Euclidean space [22]. Moreover, the uniformity of lattices suggest

that analysis is more straightforward. We provide a brief summary of pertinent results here, with a more detailed discussion found in Appendix 3A2.

The one- and two-dimensional AM/QAM designs given previously are subsets of the lattices designated $\mathbf{Z}^1$ and $\mathbf{Z}^2$, respectively, the set of all points in one and two dimensions having integer-valued coordinates. (Technically, the constellations shown are translated to be symmetric about the origin, but this does not fundamentally affect the lattice properties.) These lattices extend to higher dimensions in obvious manner and are designated by $\mathbf{Z}^N$, but provide no really interesting results for signal design by themselves. (As a base for coded transmission, these lattices are more useful, however.)

The two-dimensional hexagonal lattice is designated $\mathbf{A}_2$ and can, as with any integer lattice, be described through vector representation of points:

$$\mathbf{s}_i = n_{i_0}\mathbf{b}_0 + n_{i_1}\mathbf{b}_1, \qquad n_{i_0}, n_{i_1} \text{ integers}, \tag{3.3.66a}$$

where $\mathbf{b}_0$ and $\mathbf{b}_1$ are basis vectors, perhaps nonorthogonal, for the lattice. For $\mathbf{A}_2$,

$$\mathbf{b}_0 = (0, 2), \qquad \mathbf{b}_1 = \left(\frac{3^{\frac{1}{2}}}{2}, \frac{1}{2}\right) \tag{3.3.66b}$$

By (3.3.66a), (n_{i_0}, n_{i_1}) define a lattice point and provide its "label." Notice with the adopted basis that the minimum Euclidean distance between lattice points is again 2.

While on the topic of two-dimensional lattices, the subset of $\mathbf{Z}^2$ consisting of integer pairs whose sum is even, or whose sum is 0 modulo 2, is designated as $\mathbf{D}_2$ and would be formed by choosing $\mathbf{b}_0 = (1, 1)$ and $\mathbf{b}_1 = (1, -1)$. This checkerboard arrangement of points can, however, be seen, upon a 45° rotation of axes, to be essentially the same lattice as $\mathbf{Z}^2$, the only real difference being a stretch factor of $2^{1/2}$. We say that $\mathbf{D}_2$ and $\mathbf{Z}^2$ lattices are ***isomorphic***, that is, have the same structure. In three dimensions the densest lattice packing is provided by the ***face-centered cubic lattice***, which is depicted in Figure 3.3.28. This lattice is slightly more dense, surprisingly, than the ***body-centered cubic lattice*** and more dense than $\mathbf{A}_2$ as well. Crystallographers have studied properties of these and other three-dimensional lattices for many years.

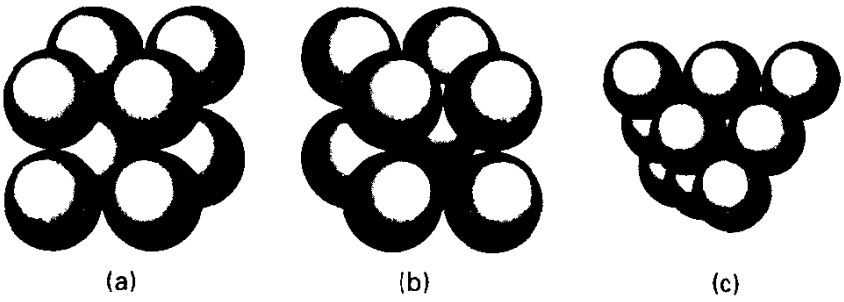

Figure 3.3.28 Three-dimensional sphere packings. (a) Simple cubical packing; (b) body-centered cubical packing; (c) face-centered cubical packing.

In four dimensions, which has more engineering appeal than three dimensions, the best lattice packing is provided by the lattice commonly designated $\mathbf{D}_4$, also known as the Schlafli lattice, formed by the set of all four-tuples of integers that have an even sum,

that is, which sum to 0, modulo 2:[17]

$$\mathbf{D}_4 = \left\{ (n_0, n_1, n_2, n_3) \,\middle|\, \sum_{k=0}^{3} n_k = 0 \bmod 2 \right\}. \tag{3.3.67a}$$

$\mathbf{D}_4$ would thus include points $(1, 1, 0, 0)$, $(1, 1, -2, 2)$, and so on.

A basis for this set is given by

$$\begin{aligned} \mathbf{b}_0 &= (2, 0, 0, 0), \\ \mathbf{b}_1 &= (1, 0, 0, 1), \\ \mathbf{b}_2 &= (0, 1, 0, 1), \\ \mathbf{b}_3 &= (0, 0, 1, 1). \end{aligned} \tag{3.3.67b}$$

With respect to this basis, the label for the lattice vector $(1, 0, -1, 0)$ is $(0, 1, 0, -1)$.

If we utilize four-dimensional constellations for M-ary signaling and compare fairly with, say, two-dimensional signaling using $\mathbf{Z}^2$, keeping the number of bits per signal-space dimension constant, we find that for large signal sets $\mathbf{D}_4$ is 1.5 dB more energy efficient than $\mathbf{Z}^2$, merely because of the efficiency of packing in higher dimensions (see Appendix 3A2).

Still better is the densest eight-dimensional lattice, designated $\mathbf{E}_8$, and known as the Gosset lattice. This lattice can be formed as follows: construct the lattice $\mathbf{D}_8$ as the set of all integer-valued 8-tuples whose coordinates sum to an even number, or whose coordinate sum is zero, modulo 2. Stretch the lattice by a factor of 2 in each dimension and call it $2\mathbf{D}_8$, which would be the set of all 8-tuples with even coordinates summing to 4. The minimum Euclidean distance between points in this stretched lattice is $2(2)^{1/2}$. It happens that we may slip a coset, or translate, of this stretched lattice, formed by adding the vector $(1, 1, 1, 1, 1, 1, 1, 1)$ to each point of $2\mathbf{D}_8$, into the interstitial space of the former stretched lattice without reducing the minimum Euclidean distance! Representative points in $\mathbf{E}_8$ are $(2, -2, 2, 2, 0, 0, 0, 0)$ and $(1, 1, 1, 3, -1, -1, -1, -1)$. Once we appropriately account for energy consumption in a large $\mathbf{E}_8$ lattice, packing theory reveals that, for fixed value of bits/signal-space dimension, another 1.5 dB is gained by the eight-dimensional arrangement over the four-dimensional arrangement. While this progression may seem unending, it must be noted that the number of nearest neighbors is rapidly increasing in the high-dimensional lattices, mitigating some of the apparent energy gain. For $\mathbf{D}_4$, the ***kissing number***, the number of nearest neighbors, is 24. In $\mathbf{E}_8$, the kissing number is 240.

Encoding of signal points in such lattices can be accomplished by table lookup or by (3.3.66). Of more importance is decoding. We transmit some selected lattice point and receive a Gaussian-noise-perturbed version, $\mathbf{r}$, a point in N-dimensional Euclidean space. ML detection corresponds to finding the signal point that is closest in Euclidean distance to $\mathbf{r}$. All the lattices cited thus far possess fast algorithms [22] for decoding a given point in R^n to the nearest lattice point, making even very large constellations with perhaps 2^{15} points realistic. For example, to find the nearest lattice point in $\mathbf{D}_4$, we round each coordinate of the received four-dimensional vector $\mathbf{r}$ to an integer and check if the sum is even. If not, we find the coordinate that was previously farthest from an

[17] This provides a description of $\mathbf{D}_N$.

integer point and round it the other way. Minor modifications are required to handle the decoding of points outside the periphery of the finite constellation. Note that, as with QAM designs, gain control is essential in proper demodulation.

Figure 3.3.29 shows the asymptotic (large signal set) relationship between the ratio of required average symbol energy E_s to squared minimum distance and the constellation size M for $\mathbf{Z}^2$, $\mathbf{D}_4$, and $\mathbf{E}_8$. Note the gain of 1.5 dB in each case. Also shown are the efficiencies of selected designs for certain M. These comparisons are fair: the energy is normalized per dimension, as is the number of signals. Thus, comparison of 16-QAM, a two-dimensional scheme, is made with a four-dimensional design having 256 points. Both have a dimensionality factor of 2 bits/signal-space dimension, and hence we claim the same spectral efficiency.

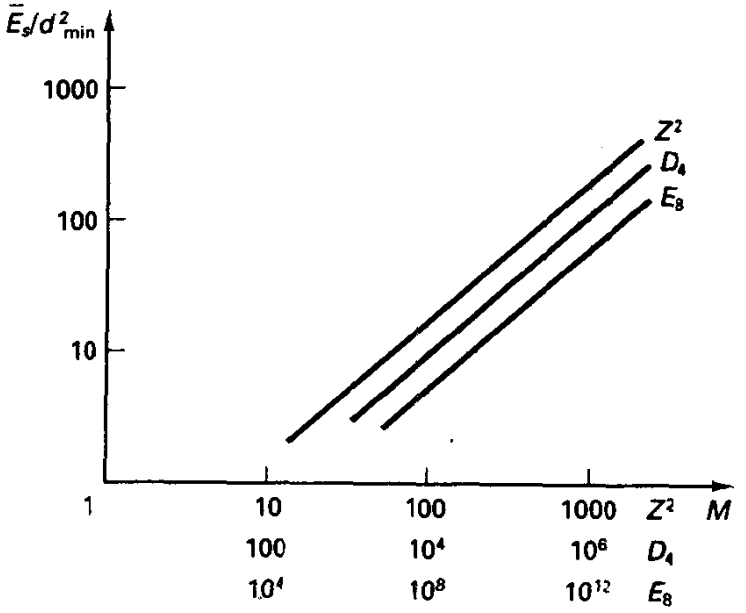

Figure 3.3.29 Packing efficiency of two, four, and eight-dimensional lattices.

Example 3.10 Design of 32-point Constellation from $\mathbf{D}_4$

To illustrate the potential of multidimensional signaling, we focus upon a 32-point design in four-dimensional signal space derived from $\mathbf{D}_4$ [23]. We include 24 points of the form $(\pm 1, \pm 1, 0, 0)$ and permutations, plus 8 points of the form $(\pm 2, 0, 0, 0)$ and permutations.[18] The normalized average energy expended per signal is $E_s = (24 \cdot 2 + 8 \cdot 4)/32 = 2.5$. At the same time, the minimum squared intrasignal distance is $d^2 = 2$. Thus, $d^2 = 0.8E_s = 4E_b$, since again each signal is presumed to convey $\log M = 5$ bits. Substituting this result into the union bound (3.3.34) (which is pessimistic regarding the multiplier) yields

$$P_s < 31Q\left[\left(\frac{2E_b}{N_0}\right)^{1/2}\right]. \tag{3.3.68}$$

which in terms of *average* energy is exponentially equivalent to antipodal signaling. However, the design here achieves a dimensional efficiency of 5 bits/4 dimensions, instead of

[18] Notice that we have eliminated the lattice point at the origin, retaining symmetry.

1 bit/1 dimension with antipodal designs. This translates into 25% better spectral efficiency for no (asymptotic) loss in energy efficiency.

Production of four- (or more) dimensional modulation may be accomplished in several ways. Most obvious is the use of two consecutive time slots of quadrature modulation, and in this sense multidimensional modulation becomes similar to the block coding techniques we will see later. Another way might be to simultaneously modulate in QAM fashion on each of two space-orthogonal polarizations of an electromagnetic wave [23]. Or we could use QAM modulation on two carriers frequency spaced to produce orthogonality. All these yield the same performance in terms of energy efficiency and spectral efficiency, if properly normalized.

Although multidimensional modulation provides somewhat modest gains over two-dimensional modulation, much of the important recent progress in coding theory for bandwidth-constrained applications has used such lattices as the modulation base for block and trellis coding. This will be reexamined in Chapters 5 and 6.

3.3.7 Summary of Energy and Spectrum Efficiency of Modulation Techniques

We have now studied numerous signaling techniques for the additive Gaussian noise environment, some of which, for example, M-ary orthogonal designs, occupy many signal-space dimensions per symbol and will be the most bandwidth consumptive. Others, for example, M-PSK or M-QAM, sacrifice energy efficiency in return for spectral economy. It is instructive now to compare the performance of these realizable schemes against the bound on this bandwidth–energy trade-off provided by the channel capacity limit of Section 2.9. This comparison is primarily useful to see the potential for still more efficient operation.

To make this comparison, we locate various signaling options studied in this section on the plot of Figure 3.3.30, a replica of Figure 2.9.7. The required E_b/N_0 for each technique is that required to produce a bit error probability of $P_b = 10^{-5}$, as found in earlier figures. There is nothing special about this performance standard, except that it is commonly used and represents good reliability for a variety of applications.

To measure the spectral efficiency of each signaling technique, we appeal to Nyquist's result that it is possible to transmit R_s samples per second, using a signal strictly band-limited to $R_s/2$ hertz, without intersymbol interference, and thus performance is identical with that of single-symbol transmission. For bandpass signaling, which is usually the case of interest, the apparent result would be that we may signal R_s symbols per second while occupying a bandwidth of R_s hertz. However, by employing quadrature modulation or, equivalently, letting the transmitted symbols be complex signal points, as in QAM/PSK, we can recoup this factor of 2 loss. Thus, consider the case of M-ary signaling within the PSK/QAM/PAM class. Letting the bit rate be R_b bps, the symbol rate becomes $R_b/\log_2 M$ sps, and the bandwidth can theoretically be as small as

$$B = \frac{R_b}{\log_2 M}, \tag{3.3.69}$$

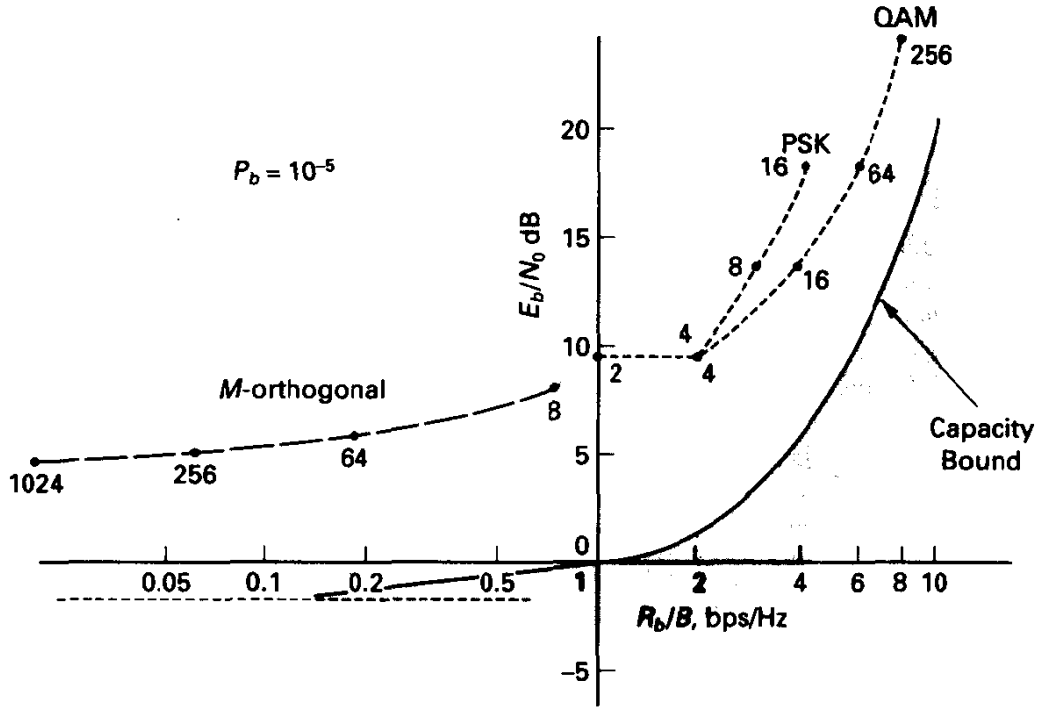

Figure 3.3.30 Energy and spectral efficiencies of standard modulation formats. All assume coherent detection.

leading to a spectral efficiency[19]

$$\frac{R_b}{B} = \log_2 M \text{ bps/Hz} \quad \text{(QAM/PAM/PSK)}. \tag{3.3.70}$$

Thus, we might say that QPSK has a spectral efficiency of 2 bps/Hz or that 64-QAM has a spectral efficiency of 6 bps/Hz. The reader should understand that these are optimistic limits; no implementable signaling method is able to achieve this spectral efficiency without intersymbol interference, and the achievable spectral efficiencies should perhaps be regarded as 25% less. More precise descriptions of power spectra are given in Section 3.7.

Consider, on the other hand, the orthogonal/biorthogonal formats. If the desired bit rate is R_b bps, then the number of orthogonal dimensions occupied by an orthogonal signal constellation is $R_b M / \log_2 M$ dimensions/second. This follows since each symbol in an M-ary orthogonal set occupies M dimensions, but the symbol rate is $R_b / \log_2 M$ sps. If these signal-space coefficients were sent at baseband, the bandwidth could be as small as $R_b M / 2 \log_2 M$ hertz without intersymbol interference. In bandpass signaling, by employing quadrature modulation, the bandwidth would also be $R_b M / 2 \log_2 M$ hertz. This points to a spectral efficiency of

$$\frac{R_b}{B} = \frac{2 \log_2 M}{M} \text{ bps/Hz} \quad \text{(orthogonal signals)}. \tag{3.3.71}$$

[19]The unit is commonly abbreviated as bps/Hz.

An alternative heuristic derivation of the bandwidth for orthogonal signaling is provided by studying M-FSK. The minimum spacing between the signal frequencies for orthogonality is $\Delta f = R_s/2$ hertz, and thus M-FSK signal frequencies span a range $MR_s/2 = R_b M/2 \log_2 M$ hertz. Although this is not equivalent to the true width of the signal's power spectrum, it is a good approximation when the number of frequencies, M, is large. Thus, the spectral efficiency is again $2 \log_2 M/M$ bps/Hz for orthogonal signaling. A factor of 2 increase in this efficiency is possible for biorthogonal signaling, since the number of dimensions occupied by the signal constellation is only $MR_b/2$.

The designs shown in Figure 3.3.30 span a large range of energy/bandwidth efficiencies, but by comparing typical modulations with the capacity bound for the band-limited Gaussian channel, it is reasonable to assert that the potential saving in E_b/N_0 is some 9 dB, while maintaining the same spectral efficiency. Closing this gap has been a principal objective of communication theorists and engineers for several decades. Important progress has been made, as will be seen in Chapters 5 and 6.

This comparison is of real designs against the channel capacity limit, admittedly somewhat tenuous. We are comparing the resources required to achieve a certain finite error probability with a limit associated with "arbitrarily small" error probability. In particular, if we had done the comparison at $P_b = 10^{-3}$ or $P_b = 10^{-9}$, our conclusions would differ somewhat. Also, the measuring of bandwidth is somewhat controversial, but the one used here is at least internally consistent and shows the correct relative positions.

3.3.8 Extension to Single-symbol Transmission on Nonideal Channels

Recall that our premise at the beginning was that the channel was ideal for the signal set adopted. If we continue with single-symbol transmission, it is really quite easy to extend our discussion to the case of nonideal linear channels, described by an impulse response $c(t)$. At the receiver, we now encounter the problem of deciding among M *distorted* signals, which might be expressed by

$$s_i'(t) = s_i(t) * c(t), \qquad i = 0, 1, \ldots, M-1, \quad -\infty < t < \infty \tag{3.3.72}$$

with * again denoting convolution. We receive one of these in the presence of additive white Gaussian noise. A procedure exactly like that followed earlier in this section would produce optimal receiver structures, including a basis function receiver, a correlation receiver, or a matched filter receiver. The latter two are the most illuminating and are shown in Figure 3.3.31, wherein we correlate with, or match to, the *distorted* signals and furthermore add bias terms, if necessary, which are related to the energy residing in the distorted signals. We denote the latter by E_i'. If the channel filter is defined to have maximum gain of 1, then $E_i' \leq E_i$, by Parseval's theorem.

Performance analysis for this situation is a direct extension of our work thus far. For example, the probability of confusing two signals sent by a distorting channel, when one-shot transmission is in effect and optimal reception is performed, is

$$P_s = Q\left[\left(\frac{E_d'}{2N_0}\right)^{1/2}\right], \tag{3.3.73}$$

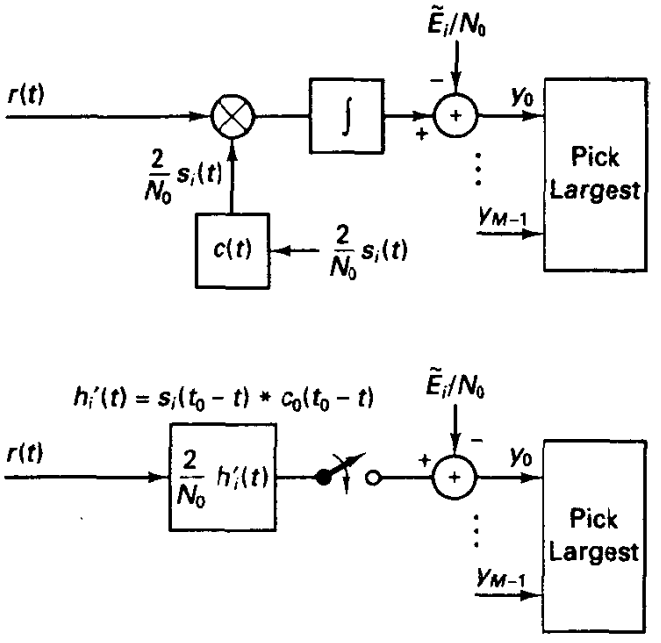

Figure 3.3.31 Correlator and matched filter detectors for one-shot distorted signal scenario. Single receiver channel shown for both.

where E_d' is the energy contained in the filtered difference signal. This is an obvious generalization of (3.3.20). This filtered difference signal energy may be much smaller than that available on an ideal channel and will depend strongly on the nature of the two signals and the impulse response of the channel. In the exercises, we illustrate the calculation by considering binary NRZ transmission through a channel whose impulse response is a pulse of width $\tau < T$.

The performance represented in (3.3.73) is sometimes known as the ***matched filter bound*** [24], for it represents a lower limit on probability of symbol error when the same signal set is employed for *sequence* transmission on a given nonideal channel. The optimal sequence processor begins with a filter matched to the distorted signal(s) and is then followed by a process of unraveling the intersymbol interference. However, the resulting probability of error for the optimal receiver can never better the performance given by (3.3.73), and the difference in energy efficiency between the actual performance and the matched filter bound reveals the real penalty exacted by the nonideal channel.

3.4 NONCOHERENT DEMODULATION OF CARRIER-MODULATED SIGNALS

To this point, we have analyzed detection under known-signal conditions, which again means that the demodulator is provided with all parameters required to perform optimal processing. This includes the amplitudes of the signals to be detected (unnecessary if all signal energies are equal) and timing parameters. In the case of carrier modulation, the assumption presumes that a phase-synchronized reference is also available, and this regime is known as ***coherent detection***. An important practical case arises when this reference phase is not known, and we model this situation by assuming that the unknown

phase angle is a random variable uniformly distributed on $[0, 2\pi)$. We refer to this regime as ***noncoherent demodulation.***

To motivate our discussion, we must understand the issues surrounding knowledge of carrier phase. It is perhaps conceivable that the receiver and transmitter could somehow synchronize their oscillators initially and depend on the relative carrier phase remaining fixed for the duration of a communication session. However, any frequency offset, no matter how small, implies a large phase error eventually. A 1-Hz offset, which corresponds to high-quality oscillators operating at 100 MHz, say, implies a phase error of 2π radians after only 1 second! Motion of the transmitter and receiver by only a fraction of a wavelength relative to each other also leads to large change in relative phase angle.

One recourse is to develop the carrier phase estimate from the received signal itself. This may be done with various forms of phase-lock-loop estimators. However, these estimators are relatively complex, the phase estimate is never perfect anyway, and the synchronizer requires an initial synchronization time for phase acquisition, leading to link inefficiency in applications where transmission is in short bursts. Sometimes it may be just as wise to dispense with trying to utilize carrier phase in the detection process.

Clearly, a receiver that knows the phase angle of the arriving signal and processes accordingly must have a performance that is at least as good as one that does not. In fact, we might expect a substantial penalty for being ignorant of carrier phase. However, we will find that this energy penalty can be made rather small with intelligent design, at least for the symbol-by-symbol detection studied here. The implications of noncoherence for coded systems may be more negative, however.

As a final introductory note, noncoherent detection is not germane to baseband transmission systems; there carrier phase knowledge is not an issue because there is simply no explicit carrier involved. Symbol timing is required in any case, however.

3.4.1 Structure of Optimal Noncoherent Demodulator

We assume the modulator can produce one of M ***carrier-modulated signals*** of the form

$$s_i(t) = a_i(t)\cos[\omega_c t + \gamma_i(t)], \qquad T_i \le t \le T_f, \tag{3.4.1a}$$

or, in complex envelope notation, we have

$$s_i(t) = \mathrm{Re}\left\{a_i(t)e^{j\gamma_i(t)}e^{j\omega_c t}\right\}, \qquad T_i \le t \le T_f. \tag{3.4.1b}$$

Here $a_i(t)$ is the (real) carrier amplitude function, and $\gamma_i(t)$ is the phase modulation process for the ith signal, both assumed known by the demodulator. If the carrier *frequency* is to be modulated, we can embed this into the phase modulation process.

The energy in a given signal is

$$E_i = \int_{T_i}^{T_f} s_i^2(t)\,dt = \frac{1}{2}\int_{T_i}^{T_f} a_i^2(t)\,dt, \tag{3.4.2}$$

assuming either $\omega_c \gg 2\pi/(T_f - T_i)$ or that $\omega_c = n2\pi/(T_f - T_i)$.

Examples of such signal sets are the following:

Binary On–Off Signaling

$$\begin{aligned} s_0(t) &= 0, \\ s_1(t) &= A\cos\omega_c t, \qquad 0 \le t \le T_s. \end{aligned} \tag{3.4.3}$$

Binary Frequency Shift Keying

$$\begin{aligned} s_0(t) &= A\cos(\omega_0 t + \theta_0), \qquad 0 \le t \le T_s, \\ s_1(t) &= A\cos(\omega_1 t + \theta_1), \end{aligned} \tag{3.4.4}$$

where ω_i and θ_i, $i = 0, 1$, are respectively the radian frequency and phases attached to two separate oscillators.

M-ary Orthogonal Signaling with Hadamard Sequences

$$s_i(t) = Ah_i(t)\cos\omega_c t, \tag{3.4.5}$$

where $h_i(t)$ is a row sequence from a binary M by M Hadamard matrix as defined in Example 3.6.

The received signal is written as[20]

$$\begin{aligned} r(t) &= s_i(t-\tau) + n(t) \\ &= s_i(t, \tau, \theta) + n(t), \end{aligned} \tag{3.4.6a}$$

where

$$s_i(t, \tau, \theta) = a_i(t-\tau)\cos[\omega_c t + \gamma_i(t-\tau) - \theta], \qquad m = 0, 1, \ldots, 2N-1, \tag{3.4.6b}$$

is merely a delayed version of the original signal with $\theta = \omega_c\tau$ modeling the unknown carrier phase shift. Under the assumption of symbol timing being available in the receiver, the effect of the transit time delay τ on the modulation components can effectively be removed from the analysis; the carrier phase θ, however, is presumed unknown. As before, the noise $n(t)$ is a sample function from a white Gaussian noise process with zero mean and noise spectral density $N_0/2$ W/Hz.

As with the model developed in Section 3.1, we assume that the phase angle θ is constant over one signaling interval, or at least very nearly so. This is generally the situation in practice unless the symbol rate is very small relative to the spectral width of the oscillator being modulated. Specifically, an oscillator whose spectral width is, say, 10 kHz has an internal phase modulation process that is highly correlated over an interval of 1 μs, the symbol interval for signaling at 1 Msps. We could not invoke the constant phase assumption, however, if this same oscillator were used for modulation at 100 sps. Spectral purity remains a technological challenge for optical communication, for current semiconductor laser sources may have optical linewidths on the order of 10^8 Hz, and bit rates typically are on this order of magnitude. The same constant phase assumption requires that any frequency uncertainty due to Doppler shift, oscillator drift,

[20]Here we explicitly show the propagation delay τ to indicate one source of the unknown carrier phase.

or the like, be reduced to a small fraction of the symbol rate. We model the variable θ as uniformly distributed on $[0, 2\pi]$, which, in the absence of prior information, is certainly the reasonable assumption.

The derivation of the optimal detector is procedurally similar to that of the known-signal case. We convert waveforms to vectors through orthonormal expansions, write likelihood functions, simplify these into a vector processor, and then let the dimensionality of the expansion become large to cast the detector as a waveform processor. The specific steps are as follows:

1. Expand $r(t)$ using an orthonormal series expansion. The expansion is in terms of the orthonormal basis set used to describe the signal, augmented by orthonormal basis functions that are in phase quadrature with the original basis set, this so that if the signal happens to arrive in exact phase quadrature with the normal basis set we obtain nonzero signal expansion coefficients nonetheless. As before, we add other orthonormal functions to complete the set. We may discard as irrelevant those expansion coefficients obtained by projection onto nonsignal bases, since again these data do not involve the hypothesis being tested in any way. We designate the relevant expansion coefficients by the vector $\mathbf{r}$. The available data are now a $2N$-vector, each of whose components is Gaussian, independent, with variance $N_0/2$, and mean values dependent on the signal index i *and* the unknown angle θ. Specifically, letting $\phi_m(t)$ represent a basis function or its phase-quadrature version, we have that the corresponding expansion coefficient for the signal component is

$$s_{im}(\theta) = \int_{T_i}^{T_f} s_i(t, \theta)\phi_m(t)\, dt, \tag{3.4.7}$$

that is, the projection of the phase-shifted signal $s_i(t, \theta)$ onto the mth basis function.

2. Express the likelihood for the ith signal as

$$f(\mathbf{r}|S_i) = \int_0^{2\pi} f(\mathbf{r}|S_i, \theta) f(\theta)\, d\theta, \tag{3.4.8a}$$

where $f(\mathbf{r}|S_i, \theta)$ is the conditional p.d.f. for the observation vector, given θ and S_i. The likelihood can then be expressed as

$$f(\mathbf{r}|S_i) = \int_0^{2\pi} f(\mathbf{r}|S_i, \theta) f(\theta) d\theta = \frac{1}{2\pi} \int_0^{2\pi} \prod_{m=0}^{2N-1} \frac{1}{(2\pi\sigma^2)^{1/2}} e^{-|r_m - s_{im}(\theta)|^2/2\sigma^2}\, d\theta. \tag{3.4.8b}$$

Note that noise independence in orthogonal dimensions has again been invoked in writing (3.4.8b). Also, conditioned on a specific signal index and θ, the signal-space projections are Gaussian.

3. Expand the likelihood function:

$$\begin{aligned} f(\mathbf{r}|S_i) &= \frac{1}{(2\pi\sigma^2)^N} \prod_{m=0}^{2N-1} e^{-r_m^2/2\sigma^2} \int_0^{2\pi} \frac{1}{2\pi} \prod_{m=0}^{2N-1} e^{-[2r_m s_{im}(\theta) + s_{im}^2(\theta)]/2\sigma^2}\, d\theta \\ &= K \int_0^{2\pi} \frac{1}{2\pi} e^{-[2\mathbf{r}\cdot\mathbf{s}_i(\theta) - \|\mathbf{s}_i(\theta)\|^2]/2\sigma^2}\, d\theta. \end{aligned} \tag{3.4.9}$$

In this last expression, we have extracted an expression common to all likelihood functions, defined as K, but this is an arbitrary scale factor and may be eliminated. In the last expression, $\mathbf{r}$ and $\mathbf{s}_i(\theta)$ are, respectively, the vectors representing the projections and the set $\{s_{im}(\theta)\}$.

4. The vector operations in the exponent of (3.4.9), such as $\mathbf{r}\cdot\mathbf{s}_i(\theta)$, can be equated with equivalent waveform operations, for example,

$$\mathbf{r}\cdot\mathbf{s}_i(\theta) = \int_{T_i}^{T_f} r(t)s_i(t,\theta)\,dt. \tag{3.4.10}$$

This follows by exactly the same argument as in Section 3.3 for known-signal derivation. Making such equivalences in (3.4.9) and recalling that $\sigma^2 = N_0/2$ gives that the optimal noncoherent detector should

$$\underset{i}{\text{maximize}} \int_0^{2\pi} \frac{1}{2\pi} \exp\left[\frac{2}{N_0}\int_{T_i}^{T_f} r(t)s_i(t,\theta)\,dt - \frac{1}{N_0}\int_{T_i}^{T_f} s_i^2(t,\theta)\,dt\right] d\theta. \tag{3.4.11}$$

The last integral in the exponent is the energy in signal i and is independent of θ, so the corresponding exponential term may be brought outside the first integral, yielding

$$\underset{i}{\text{maximize}}\ e^{-E_i/N_0} \int_0^{2\pi} \frac{1}{2\pi} \exp\left[\frac{2}{N_0}\int_{T_i}^{T_f} r(t)s_i(t,\theta)\,dt\right] d\theta. \tag{3.4.12}$$

We observe that the inner integral is a correlation integral, given a fixed θ, and this correlation is to be exponentiated and then averaged over θ to determine the decision statistic for message S_i. Fortunately, the signal processing is much simpler.

To see how to perform (3.4.12) more feasibly, we define

$$z_{c_i} = \int_{T_i}^{T_f} r(t)s_i(t)\,dt \tag{3.4.13a}$$

and

$$z_{s_i} = \int_{T_i}^{T_f} r(t)s_i\left(t, \frac{\pi}{2}\right) dt, \tag{3.4.13b}$$

where

$$s_i\left(t, \frac{\pi}{2}\right) = a_i(t)\cos\left[\omega_c t + \gamma_i(t) - \frac{\pi}{2}\right] = a_i(t)\sin[\omega_c t + \gamma_i(t)]. \tag{3.4.13c}$$

that is, a quadrature-phase-shifted version of the ith signal.[21] Then (3.4.12) becomes

$$\underset{i}{\text{maximize}}\ e^{-E_i/N_0} \int_0^{2\pi} \frac{1}{2\pi} \exp\left[\frac{2(z_{c_i}\cos\theta - z_{s_i}\sin\theta)}{N_0}\right] d\theta. \tag{3.4.14}$$

[21] The absolute phase of the reference signals is not important as long as they remain in phase quadrature.

By employing a rectangular-to-polar conversion of coordinates,

$$z_i = ({z_{c_i}}^2 + {z_{s_i}}^2)^{1/2} \tag{3.4.15a}$$

and

$$\delta = \tan^{-1}\left(\frac{z_{s_i}}{z_{c_i}}\right), \tag{3.4.15b}$$

we see that the decision rule (3.4.14) may be written as

$$\underset{i}{\text{maximize}}\ e^{-E_i/N_0}\frac{1}{2\pi}\int_0^{2\pi}\exp\left[\frac{2z_i}{N_0}\cos(\delta+\theta)\right]d\theta. \tag{3.4.16}$$

The integral in (3.4.16) is related to a special function $I_0(x)$ known as the ***zeroth-order modified Bessel function of the first kind***, defined as

$$I_0(x) \triangleq \frac{1}{2\pi}\int_0^{2\pi}\exp[x\cos\beta]\,d\beta. \tag{3.4.17}$$

$I_0(x)$ has the graph shown in Figure 3.4.1 and in particular is monotone increasing in its argument. The reader is referred to Abramowitz and Stegun [25] for a thorough description of this function, including series expansions, and approximations for large- and small-argument cases.

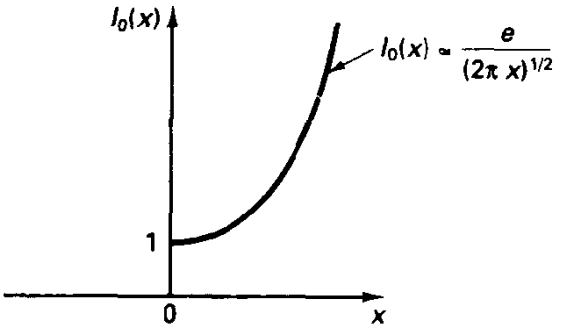

Figure 3.4.1 Modified Bessel function $I_0(x)$.

Since $\cos(x)$ is periodic in its argument and the integration in (3.4.16) is over one period, the rule of (3.4.16) can be expressed as

$$\underset{i}{\text{maximize}}\ e^{-E_i/N_0}I_0\left(\frac{2z_i}{N_0}\right). \tag{3.4.18}$$

Upon taking the logarithm, a monotone-increasing function of its argument, we may equivalently state the rule as

$$\boxed{\underset{i}{\text{maximize}}\ \log_e I_0\left(\frac{2z_i}{N_0}\right) - \frac{E_i}{N_0}.} \tag{3.4.19}$$

If all the signal energies are equal, which is typical in noncoherent detection settings, we can eliminate the bias term in (3.4.19) and just as well maximize z_i or equivalently z_i^2, again because of monotonicity of $\log_e I_0(x)$. The optimal noncoherent receiver

then has the form shown in Figure 3.4.2. We remark that for each signal two waveform correlations are required, plus squaring, so the complexity is somewhat larger than for the coherent receiver, at some disparity with conventional thought. (The noncoherent receiver is, of course, spared the need to acquire phase estimates.)

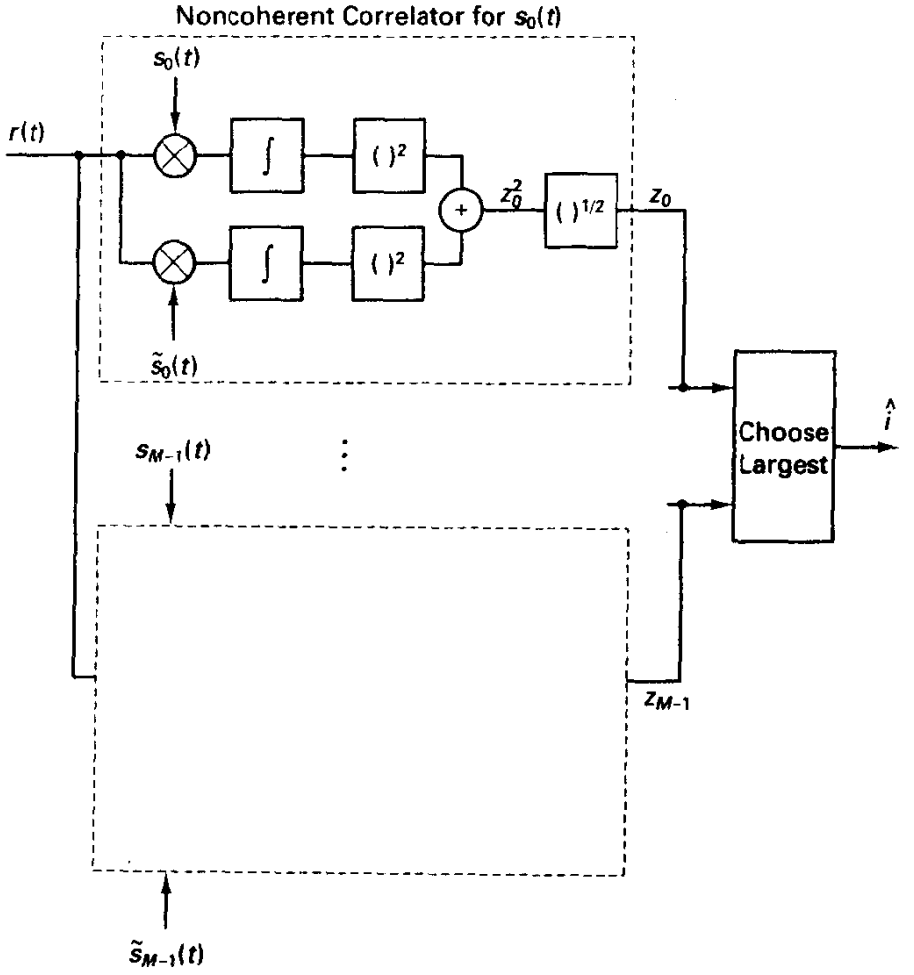

Figure 3.4.2 Block diagram of optimal noncoherent receiver, correlator form, equal symbol energies.

In passing, we note that if the demodulator has some knowledge of the signal phase, but not exact knowledge as in Section 3.3, a variation on the present receiver can be designed to optimally combine the two quadrature correlator channels [26, 27]. Practical implementations seem to use either the known-phase processor, even though phase may not be perfectly known, or fall back to the completely unknown phase processor.

Other forms of this receiver are possible, as was the case with coherent detection. In particular, since all signals contain the same $\cos(\omega_c t)$ dependency, we may develop a receiver that does carrier multiplication by $\cos(\omega_c t)$ and by $\sin(\omega_c t)$ and then do the bulk of the processing with baseband, perhaps digital, circuitry. (Exercise 3.4.3 explores this for one signaling example.)

Another common form is the ***bandpass matched filter*** form, especially appropriate for the M-ary FSK case. Here we use M parallel matched filters, with impulse responses

$$h_i(t) = \frac{2}{N_0} s_i(T_f - t), \qquad T_i \le t \le T_f. \tag{3.4.20}$$

and sample the ***envelope*** of the filters' outputs at $t = T_f$. This operation produces the same decision statistics z_i as the receiver of Figure 3.4.2, since the envelope of a bandpass signal is defined as the root-sum-square value of its quadrature components. Figure 3.4.3 illustrates the noncoherent matched filter implementation. As when choosing among coherent receiver structures, design issues would dictate which form of the noncoherent receiver is preferred.

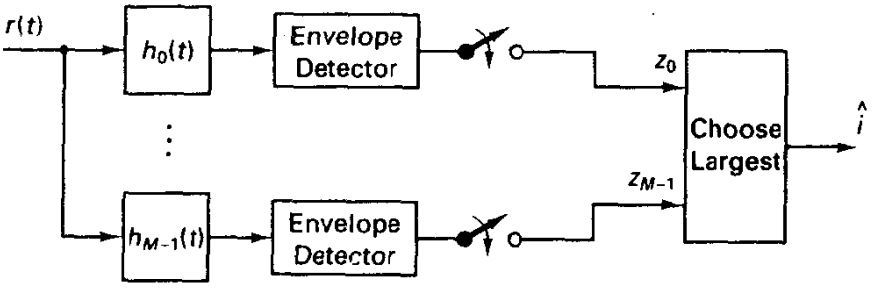

Figure 3.4.3 Optimal noncoherent receiver, matched filter form, equal symbol energies.

3.4.2 Performance Analysis for Noncoherent Demodulation of Binary Orthogonal Signals

Given two carrier-modulated signals with equal energies and prior probabilities, Figure 3.4.2 reduces to the receiver shown in Figure 3.4.4. We shall first treat the case of *binary* orthogonal signals. Our emphasis on orthogonal signals is based on the fact that this choice provides the smallest probability of error among the class of binary signals, provided phase is unknown and peak energy is constrained [26].

To analyze the error probability, we may assume without loss of generality that $s_0(t)$ is the transmitted signal and that the unknown phase angle θ at the receiver is zero, since performance is invariant to θ. First, consider the statistics x_1 and y_1 in Figure 3.4.4. Since $s_1(t)$ is orthogonal to $s_0(t)$, the random variables X_1 and Y_1 will both have zero mean. Each has variance $\sigma^2 = 2E_s/N_0$ as before. Furthermore, X_1 and Y_1 are independent Gaussian variates, since $s_i(t)$ and $\tilde{s}_i(t)$ are orthogonal. The root-sum square of independent Gaussian variates is Rayleigh distributed, as developed in Chapter 2. Thus,

$$f(z_1|S_0) = \frac{z_1}{\sigma^2} e^{-z_1^2/2\sigma^2}, \qquad z_1 \ge 0. \tag{3.4.21}$$

The only difference when considering Z_0 is that X_0 has a mean value given by $\mu = 2E_s/N_0$. The density function for

$$Z_0 = (X_0^2 + Y_0^2)^{1/2} \tag{3.4.22}$$

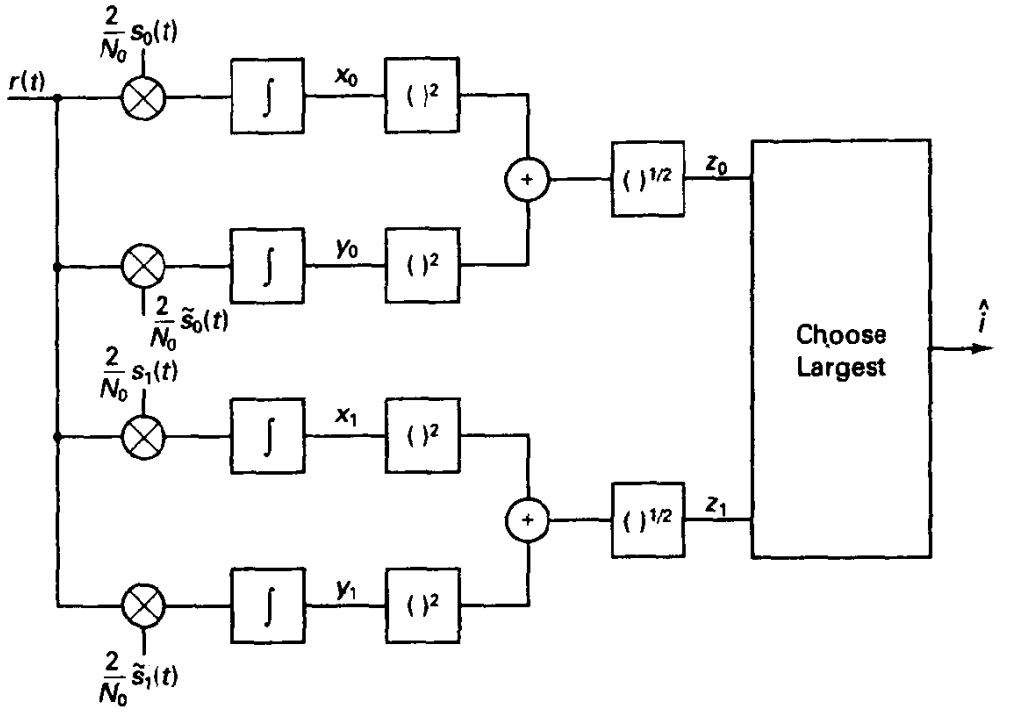

Figure 3.4.4 Noncoherent receiver for $M = 2$ signals.

has the Rician form

$$f(z_0|S_0) = \frac{z_0}{\sigma^2} I_0\left(\frac{\mu z_0}{\sigma^2}\right) e^{-(z_0^2+\mu^2)/2\sigma^2}, \qquad z_0 \geq 0. \tag{3.4.23}$$

We encountered these two density functions in Chapter 2, and a sketch of the probability density functions is found in Figure 2.2.5.

The probability of error, given that message S_0 is sent, is

$$P(\epsilon|S_0) = P(Z_1 \geq Z_0|S_0) = \int_0^\infty \int_{z_0}^\infty f(z_0, z_1|S_0)\, dz_1\, dz_0. \tag{3.4.24}$$

The random variables Z_0 and Z_1 are independent because their respective noise variables are independent, which in turn follows from the orthogonality of the two signals. In Example 2.7, we evaluated the integral of (3.4.24) and found it to have the simple result that

$$P(\epsilon|S_0) = \frac{1}{2} e^{-\mu^2/4\sigma^2}, \tag{3.4.25}$$

where again $\mu = 2E_s/N_0$ and $\sigma^2 = 2E_s/N_0$. By symmetry, $P_s = P(\epsilon|S_0) = P(\epsilon|S_1)$, and substitution for μ and σ^2 gives

$$\boxed{P_s = \frac{1}{2} e^{-E_b/2N_0}, \qquad \text{(binary orthogonal, noncoherent detection, AWGN)}} \tag{3.4.26}$$

(We have also used $E_b = E_s$ for the binary case.) It is perhaps surprising that, despite the more complex receiver compared to the coherent case and the more exotic probability density functions involved in the derivation, the expression for error probability has a very simple analytical form.

We should now compare the performance of noncoherent detection of binary orthogonal signals with that of coherent detection. At $P_s = 10^{-5}$, noncoherent signaling, upon solution of (3.4.26), requires $E_b/N_0 = 13.4$ dB, while coherent detection necessitates 12.6 dB. This rather small loss in efficiency is purely attributable to the lack of phase information in the demodulation. The two options are, in fact, exponentially equivalent, as may be seen by substituting the upper bound for the Q-function (2.2.15b) in the expression for coherent detection of orthogonal signals.

Insight into the large SNR equivalence of coherent and noncoherent demodulation can be obtained by noting that the decision statistic Z_0, conditioned on transmission of message S_i, is a Rician random variable. For large SNR, this random variable becomes nearly Gaussian, with mean $\mu = 2E_s/N_0$ and variance $\sigma^2 = 2E_s/N_0$ as well. Z_1 is Rayleigh distributed, but in the positive tail region the p.d.f. varies exponentially as $e^{-z_1^2/2\sigma^2}$. Thus, for large SNR the hypothesis testing problem is nearly that of deciding between two Gaussian distributions with different means. This test has error probability given by the coherent demodulation result.

A less favorable view toward noncoherent detection is that the *best noncoherent binary scheme* is about 3.8 dB inferior at error probability 10^{-5} to the *best coherent binary scheme* (antipodal signaling). The real energy penalty for not knowing carrier phase is thus more than a factor of 2 in the $M = 2$ case. Indeed, we would not expect to see binary orthogonal signaling with coherent demodulation in practice, for if phase synchronization is available, an immediate 3-dB gain is available by using antipodal signals. We are about to see, however, that the efficiency difference between noncoherent and coherent detection schemes gradually becomes small as M increases.

3.4.3 Performance Analysis of Noncoherent Detection of M-ary Orthogonal Signals

The extension to the M-ary orthogonal case is now straightforward, although the resulting error probability expressions are less compact. The optimal receiver now includes M noncoherent correlators acting in parallel, generating random variables $Z_0, Z_1, \ldots, Z_{M-1}$, and the demodulator selects the index of the largest statistic.

As before, we assume $s_0(t)$ is transmitted. By symmetry, the symbol error probability P_s will be just the conditional error probability, $P(\epsilon|S_0)$. As in the binary case, Z_0 will have a Rician density, while the remaining Z_i will have Rayleigh densities. All variables are independent.

We seek the probability that *all* Z_i are less than Z_0, which is the probability of correct decision. We attack this by fixing $Z_0 = z_0$, calculating the conditional result, and then averaging over z_0. First,

$$\begin{aligned} P(C|S_0, z_0) &= P\ (\text{ all } Z_i \le z_0, i = 1, 2, \ldots, M-1|S_0) \\ &= \left(\int_0^{z_0} \frac{z}{\sigma^2} e^{-z^2/2\sigma^2} dz\right)^{M-1} \\ &= \left[1 - e^{-z_0^2/2\sigma^2}\right]^{M-1} \end{aligned} \tag{3.4.27}$$

Now averaging against the Rician p.d.f. for Z_0, we obtain

$$P(C|s_0) = \int_0^\infty \frac{z_0}{\sigma^2} I_0\left(\frac{\mu z_0}{\sigma^2}\right) \exp\left[-\left(\frac{z_0^2 + \mu^2}{2\sigma^2}\right)\right]\left[1 - e^{-z_0^2/2\sigma^2}\right]^{M-1} dz_0. \quad (3.4.28)$$

The bracketed term raised to the power $(M - 1)$ in (3.4.28) may be expanded using the binomial expansion. Then, integrating term by term and applying the same result developed in the binary case (Example 2.7), we obtain

$$P_s = 1 - P(C) = \sum_{j=1}^{M-1} \frac{(-1)^{j+1}}{j+1} C_j^{M-1} e^{-jE_s/(j+1)N_0}, \quad (3.4.29)$$

which may be computed without resort to special functions.

Figure 3.4.5 illustrates the dependence of P_s on M and E_b/N_0, again showing that energy efficiency improves with increasing M. Also, note that by comparing Figures 3.3.17 and 3.4.5, for large M the noncoherent detection penalty becomes small. For example, to obtain $P_s = 10^{-5}$ with $M = 64$ and coherent detection requires $E_b/N_0 =$ 6.5 dB, while iterative solution of (3.4.29) for noncoherent detection yields $E_b/N_0 =$ 6.9 dB, a difference of only 0.4 dB. (We could correctly argue that we should instead be comparing better coherent schemes, that is, biorthogonal designs, which could not be employed with noncoherent detection, but the incremental gain is still small for large M.)

The bit error probability, P_b, can be related to symbol error probability, P_s, in exactly the same way as we did for coherent detection:

$$P_b = \frac{M}{2(M-1)} P_s. \quad (3.4.30)$$

This again follows from simple counting arguments.

We may correctly infer that as $M \to \infty$ the efficiency of M-ary orthogonal signaling with noncoherent detection also approaches the channel capacity limit for the AWGN channel. Specifically, by grouping message bits together into M-ary orthogonal symbols, as long as $E_b/N_0 > -1.6$ dB, arbitrarily small probability of symbol (message) error can be achieved as M increases. This reveals that lack of phase information actually is not fundamentally detrimental. The problem with this approach to efficient communication is again one of exorbitant complexity.

Example 3.11 8-ary FSK Transmission

Suppose that a radio communications link for a wireless factory network is designed to transmit data at a rate of 256 kbps on a carrier frequency around 1800 MHz. One option for modulation is 8-ary FSK. Let's design the signaling parameters and analyze the performance.

Information is transmitted in 3-bit chunks, so the required symbol rate will be $R_s =$ 256/3 = 85.3 ksps. Every 3-bit symbol produces a certain frequency, near 1800 MHz, either by selecting from a bank of oscillators or, more likely, by frequency modulating a single oscillator. (The modulation is normally done at a lower frequency; then the signal is "up-converted.") For the set of eight signals to be mutually orthogonal, we must select a signal frequency spacing $2\Delta f$ equaling some multiple of R_s when the detection is not phase coherent.[22] Thus, picking the minimum separation, we have a signal set that spans

[22] It is a curious fact that when phase coherent reception is adopted the spacing can be half as large and orthogonality is still maintained; see Exercise 3.4.5.

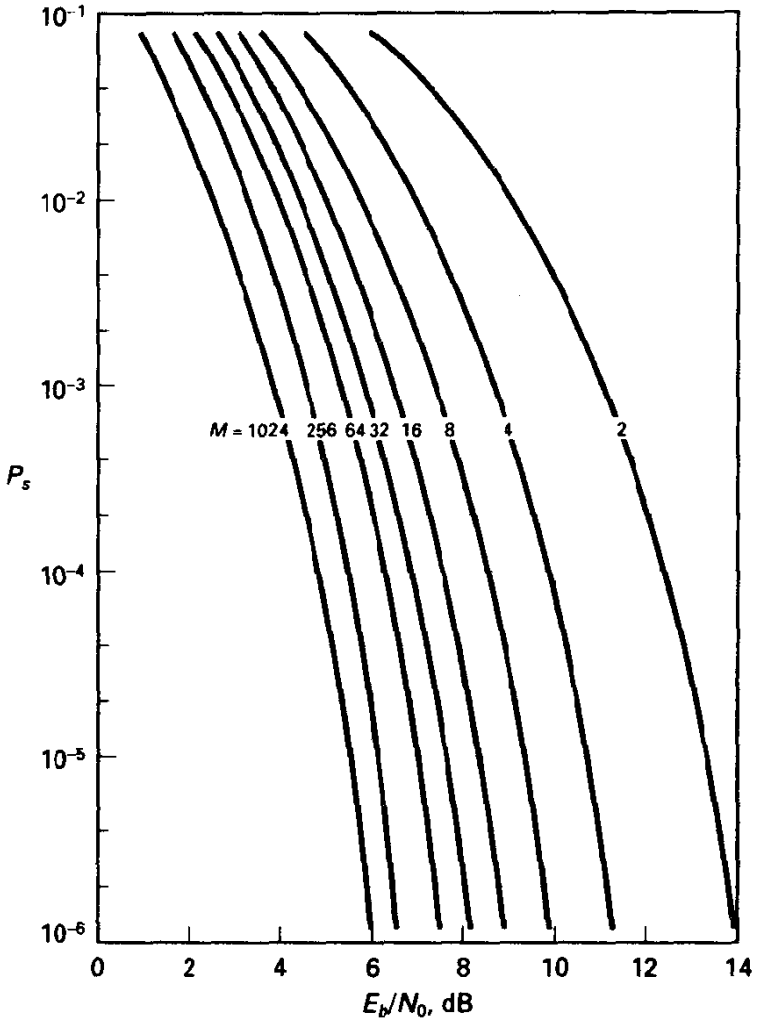

Figure 3.4.5 Symbol error probability for noncoherent detection of M-ary orthogonal signals.

a region of $7R_s = 597$ kHz. The exact form of the power spectrum is complicated, depending on whether phase continuity exists in the modulation process, but the bandwidth is roughly $8R_s$.

To achieve a bit error probability of $P_b = 10^{-6}$ requires a symbol error probability $P_s = 1.75 \cdot 10^{-6}$, by (3.4.30), and from Figure 3.4.5, we determine that the necessary $E_b/N_0 \approx 10$ dB. If the known noise spectral density at the input to the demodulator is $N_0/2 = 10^{-10}/2$, then the required signal power at the same point in the receiver is

$$P_r = \frac{E_b}{T_b} = 10^{-9}(256 \cdot 10^3) = 0.26 \text{ mW}. \tag{3.4.31}$$

Several demodulator implementations are conceivable, but the easiest is probably a bank of bandpass filters, approximating matched filters, operating at a receiver intermediate frequency of perhaps 5 MHz with frequency spacing of 85.3 kHz. Envelope detection,

sampling, and choice of the largest statistic provides the symbol decisions. Another implementation involves conversion of the signal to baseband, followed by sampling and calculation of the DFT. Decision is in favor of the frequency producing the largest magnitude-squared result.

3.5 PHASE COMPARISON OR DIFFERENTIALLY COHERENT DEMODULATION OF PSK

We have just seen that certain sets of signals may be detected without a synchronized carrier phase reference, provided the unknown channel phase is slowly varying. It seems paradoxical to consider this for PSK signaling, but a noncoherent receiver can indeed be implemented. The key is to encode information in phase differences and then use phase differencing at the receiver to demodulate. Encoding is in fact the same as for differentially encoded coherent PSK, as described in Section 3.3.4, but no phase-tracking loop is used at the receiver. Instead, only reasonably accurate frequency synchronization is required. This general approach is generally referred to as ***M*-ary DPSK** in the literature.[23] In the binary case, we will find that DPSK is only slightly less efficient than PSK, providing a means of doing noncoherent detection with near-antipodal efficiency.

In M-ary DPSK, we let the carrier phase angle of the modulator for the nth symbol interval be specified by the recursion

$$\theta_n = \left(\theta_{n-1} + x_n \frac{2\pi}{M}\right), \qquad \text{modulo } 2\pi, \tag{3.5.1}$$

where x_n is a modulator input symbol contained in $\{0, 1, \ldots, M-1\}$. This same recursion was introduced in Section 3.3.4 for similar reasons.

The transmitted signal is the PSK waveform

$$s(t) = \left(\frac{2E_s}{T_s}\right)^{1/2} \cos(\omega_c t + \theta_n), \qquad nT_s \le t \le (n+1)T_s. \tag{3.5.2}$$

Thus, we implement M-ary PSK modulation, but with the *phase differences* $\delta_n = \theta_n - \theta_{n-1}$, modulo 2π, defined by the symbol sequence $\{x_n\}$. The differentially encoded signal has the same statistical properties as the sequence x_n, and thus the spectral properties of M-DPSK are identical with those of M-PSK.

This mapping technically violates the earlier definition that modulation is a memoryless process—here the current phase apparently depends on all the previous symbols. However, the memory induced here is such a simple form that we will include DPSK in our list of modulations. In particular, the sets of waveforms produced by M-ary PSK and DPSK modulators are the same.

[23] The nomenclature varies: some systems described as DPSK are in fact coherently-detected, differentially-decoded PSK.

3.5.1 Structure of Optimal Demodulator

At the receiver, due to an unknown (but assumed fixed) phase offset θ and the addition of white Gaussian noise, we observe

$$r(t) = \left(\frac{2E_s}{T_s}\right)^{1/2} \cos(\omega_c t + \theta_n + \theta) + n(t). \tag{3.5.3}$$

We first develop the DPSK demodulator from intuitive reasoning. As shown in Figure 3.5.1, using quadrature correlation with $\cos(\omega_c t)$ and $\sin(\omega_c t)$ to produce the in-phase and quadrature estimates of the signal phasor, followed by an arctangent operation, the phase angle of the received signal over one symbol can be estimated:[24]

$$\gamma_n = \tan^{-1}\left(\frac{r_{sn}}{r_{cn}}\right) \tag{3.5.4}$$

This signal phase, in the absence of noise, is the sum of the unknown reference phase, θ, and the modulation phase, θ_n. If θ does not change appreciably over two symbols, we may form the differences of the measured phase, derived from consecutive intervals, to provide an estimate of the phase difference δ_n, which conveys the information. To see the basic principle, write $\gamma_n = \theta_n + \theta + \beta_n$, where β_n denotes the phase error due to additive noise. A similar expression applies at time $n - 1$. The estimated phase difference is

$$\hat{\delta}_n = \gamma_n - \gamma_{n-1} = \theta_n - \theta_{n-1} + \beta_n - \beta_{n-1} = \delta_n + \beta_n - \beta_{n-1}. \tag{3.5.5}$$

(All additions and subtractions are modulo 2π.) Thus, the unknown phase angle θ vanishes, and the data symbol may be correctly recovered by quantizing $\hat{\delta}_n$ into one of M equiangular decision zones, using the rule (3.5.1), provided the difference of the measurement errors is less than π/M in magnitude. Notice the phase estimate derived from the previous interval is always employed to decide in the present interval, and

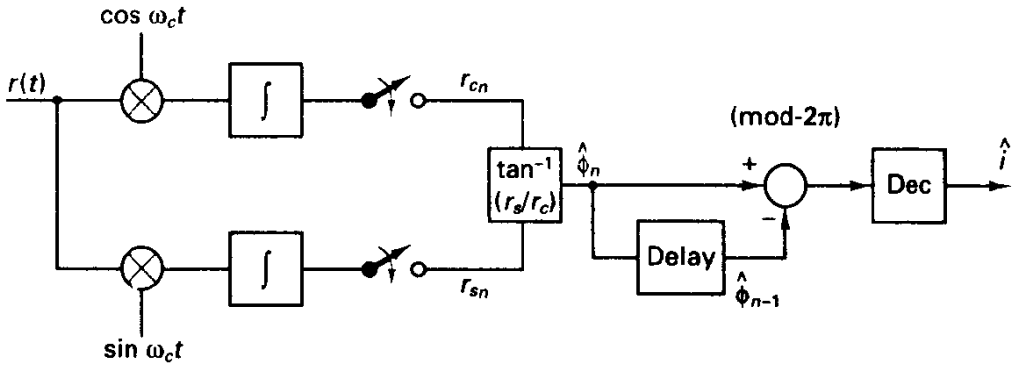

Figure 3.5.1 General M-DPSK receiver.

[24]This happens to be the maximum-likelihood estimate [26].

only one start-up symbol is needed to begin the process. An example of encoding and demodulation for $M = 2$ is provided in Figure 3.5.2.

Information Sequence		0	1	1	0	1
Carrier Phase at Modulator Output	0	0	π	0	0	π
Carrier Phase at Demodulator Output (no noise)	0 + θ	0 + θ	π + θ	0 + θ	0 + θ	π + θ
Phase Difference		0	π	π	0	π
Data Output		0	1	1	0	1

Figure 3.5.2 Encoding/decoding example for binary DPSK.

Although this signal processing is intuitively well grounded, it is possible to obtain the adopted receiver directly from principles of optimal noncoherent detection. We formulate the decision problem as a problem in unknown phase reception where the observation consists of *two* consecutive symbol intervals. M hypotheses are to be tested, each corresponding to a certain phase difference. The optimal noncoherent receiver would, as in Section 3.4, form noncoherent correlations for each of the M hypotheses by integrating over two symbol intervals in each quadrature arm and then squaring and summing. The decision is then in favor of that noncoherent correlation producing the largest statistic, as in Section 3.4.

To simplify the structure of such a receiver, we first express the two quadrature correlations obtained by $2T_s$-second integration for each signal hypothesis:

$$\begin{aligned} x_{i,n} &= \int_{(n-2)T_s}^{(n-1)T_s} r(t)\cos\omega_c t\,dt + \int_{(n-1)T_s}^{nT_s} r(t)\cos(\omega_c t + \delta_{i,n})\,dt, \\ y_{i,n} &= \int_{(n-2)T_s}^{(n-1)T_s} r(t)\sin\omega_c t\,dt + \int_{(n-1)T_s}^{nT_s} r(t)\sin(\omega_c t + \delta_{i,n})\,dt, \end{aligned} \tag{3.5.6}$$

where now $\delta_{i,n}$ denotes the ith hypothesized phase increment at time n. The decision statistic for the ith hypothesis then becomes, from Section 3.4,

$$z_{i,n}^2 = x_{i,n}^2 + y_{i,n}^2, \qquad i = 0, 1, \ldots, M-1. \tag{3.5.7}$$

Simple trigonometric manipulation shows that these decision statistics are related to the quadrature correlator variables r_{c_n} and r_{s_n} in Figure 3.5.1 by

$$z_{i,n}^2 = \left[r_{c_{n-1}} + r_{c_n}\cos\delta_{i,n} - r_{s_n}\sin\delta_{i,n}\right]^2 + \left[r_{s_{n-1}} + r_{s_n}\cos\delta_{i,n} + r_{c_n}\sin\delta_{i,n}\right]^2. \tag{3.5.8a}$$

By invoking phasor notation for the two consecutive measurements, we can see that $z_{i,n}^2$ is equivalent to

$$z_{i,n}^2 = \left|\mathbf{r}_n + \mathbf{r}_{n-1}e^{+j2\pi i/M}\right|^2, \qquad i = 0, 1, \ldots, M-1, \tag{3.5.8b}$$

where $\mathbf{r}_n = r_{c_n} + jr_{s_n}$ represents the integrator output at time n. Equation (3.5.8b) can be interpreted as rotating the previous phasor by the hypothesized phase advance and then summing with the current phasor and forming the magnitude squared. Upon expanding the magnitude-squared expression in (3.5.8b) and eliminating common terms for each statistic, we may equivalently

$$\underset{i}{\text{maximize}}\ \text{Re}\left\{\mathbf{r}_n\mathbf{r}_{n-1}^* e^{-j2\pi i/M}\right\}. \tag{3.5.9a}$$

If we interpret $\mathbf{r}_n$ as a vector in the plane and $\mathbf{r}_{n-1}^* e^{j2\pi i/M}$ as another, the decision should

$$\underset{i}{\text{maximize}}\ \mathbf{r}_n \cdot \left(\mathbf{r}_{n-1}e^{+j2\pi i/M}\right), \tag{3.5.9b}$$

which is just the vector inner or dot product between the current measurement and the rotated previous measurement vectors. Thus, optimal processing can be reinterpreted as follows: rotate the first phasor by the hypothesized phase advance; then compute the vector inner product with the next phasor and decide in favor of the largest.

Still another formulation of the optimal differential detector follows from applying Euler's relation to (3.5.9a), yielding

$$\underset{i}{\text{maximize}}\ |\mathbf{r}_n||\mathbf{r}_{n-1}|\cos\left(\gamma_n - \gamma_{n-1} - \frac{2\pi i}{M}\right), \tag{3.5.10}$$

from which it becomes clear that the *magnitudes* of the phasors are irrelevant, and only $\delta_n = \gamma_n - \gamma_{n-1}$ is important. Thus, the phase-differencing demodulator is optimal when the decision is based on two consecutive symbol intervals.

For small M, the DPSK receiver can be implemented in a manner that avoids much of the complexity of Figure 3.5.1, in particular the inverse-tangent operation. In the binary DPSK case, (3.5.10) simplifies to testing whether the measured phase difference δ_n exceeds $\pi/2$ in magnitude. If so, then the decision 1 is produced; else 0 is decided. Equivalently, we test whether the vector inner product of two consecutive (nonrotated) phasors is negative or positive. In terms of the data produced within the demodulator, we have the test

$$r_{c_n}r_{c_{n-1}} + r_{s_n}r_{s_{n-1}} \underset{1}{\overset{0}{\gtrless}} 0, \tag{3.5.11}$$

which defines the binary receiver of Figure 3.5.3a. Similarly, in the $M = 4$ case, the processing may be interpreted as sign tests on the vector inner product and cross product of consecutive measurements (Exercise 3.5.3).

An alternative binary DPSK receiver is shown in Figure 3.5.3b, involving a front-end filter matched to the signal over one interval, that is, a constant phase sinusoid of duration T_s seconds, followed by a delay line and a sampled phase detector. (It is imperative that the delay be nearly equivalent to a multiple of 2π radians at the operating center frequency of the detector, certainly an implementation difficulty.)

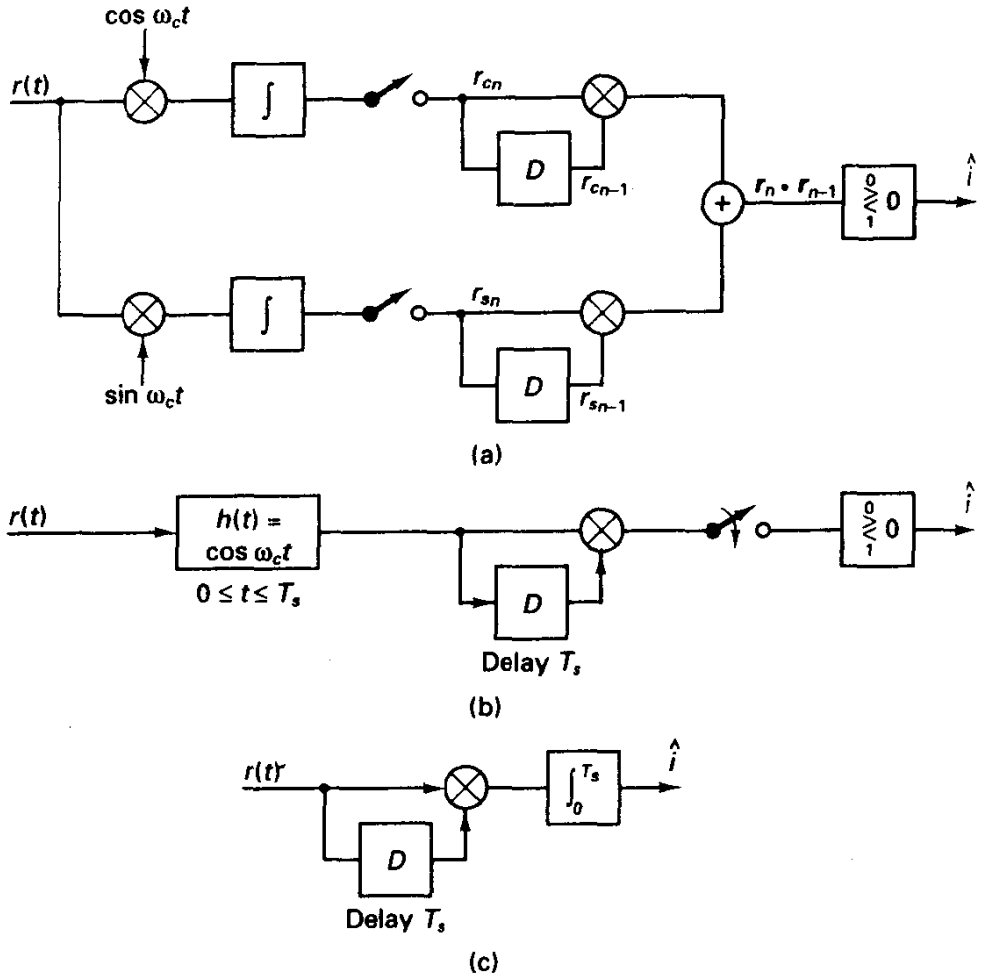

Figure 3.5.3 Two implementations of binary DPSK demodulator. (a) baseband inner product form; (b) matched filter/delay line form; (c) wrong implementation of binary DPSK demodulator.

In the detector of Figure 3.5.3b, all essential noise filtering is performed by the matched filter. Prevalent in textbooks, but suboptimal, is the receiver shown in Figure 3.5.3c, which reverses the order. Notice that the phase detection step (multiplication of two bandpass signals) indicated in Figure 3.5.3b is nonlinear with respect to the input, and we simply cannot commute the order of the operations. Although this receiver produces correct decisions for sufficiently high SNR, its performance is substantially worse than the optimal DPSK receiver at SNRs of interest.

3.5.2 Performance Evaluation for *M*-DPSK

To evaluate the demodulator error probability, we consider first the *binary* case. One helpful way of visualizing binary DPSK is as a binary orthogonal design lasting $2T_s$ seconds. Each interval uses the previous bit as a phase reference, so we might write the